NUMERICAL AND EXPERIMENTAL INVESTIGATION OF RADAR ABSORBING PERFORMANCE OF COMPOSITE MATERIALS WITH FREQUENCY SELECTIVE SURFACE

A THESIS SUBMITTED TO
THE GRADUATE SCHOOL OF NATURAL AND APPLIED SCIENCES
OF
MIDDLE EAST TECHNICAL UNIVERSITY

BY

BUSE SUBAŞI

IN PARTIAL FULFILLMENT OF THE REQUIREMENTS
FOR
THE DEGREE OF MASTER OF SCIENCE
IN
METALLURGICAL AND MATERIALS ENGINEERING

NOVEMBER 2022

Approval of the thesis:

NUMERICAL AND EXPERIMENTAL INVESTIGATION OF RADAR ABSORBING PERFORMANCE OF COMPOSITE MATERIALS WITH FREQUENCY SELECTIVE SURFACE

submitted by **BUSE SUBAŞI** in partial fulfillment of the requirements for the degree of **Master of Science** i**n Metallurgical and Materials Engineering, Middle East Technical University** by,

Prof. Dr. Halil Kalıpçılar
Dean, Graduate School of **Natural and Applied Sciences** _____

Prof. Dr. Ali Kalkanlı
Head of the Department, **Metallurgical and Materials Engineering** _____

Assoc. Prof. Dr. Caner Şimşir
Supervisor, **Metallurgical and Materials Eng., METU** _____

Assoc. Prof. Dr. Bektaş Çolak
Co-Supervisor, **Physics, Gebze Technical University** _____

Examining Committee Members:

Prof. Dr. C. Hakan Gür
Metallurgical and Materials Eng, METU _____

Prof. Dr. H. Emrah Ünalan
Metallurgical and Materials Eng, METU _____

Prof. Dr. Amdulla Mekhrabov
Metallurgical and Materials Eng, METU _____

Assoc. Prof. Dr. Caner Şimşir
Metallurgical and Materials Eng, METU _____

Prof. Dr. Bulat Z. Rami
Physics, Gebze Technical University _____

Date: 18.11.2022

I hereby declare that all information in this document has been obtained and presented in accordance with academic rules and ethical conduct. I also declare that, as required by these rules and conduct, I have fully cited and referenced all material and results that are not original to this work.

Name Last name : Buse Subaşı

Signature :

ABSTRACT

NUMERICAL AND EXPERIMENTAL INVESTIGATION OF RADAR ABSORBING PERFORMANCE OF COMPOSITE MATERIALS WITH FREQUENCY SELECTIVE SURFACE

Subaşı, Buse
Master of Science, Metallurgical and Materials Engineering
Supervisor : Assoc.Prof.Dr.Caner Şimşir
Co-Supervisor: Assoc. Prof. Dr. Bektaş Çolak

November 2022, 90 pages

Materials having radar absorbing property show critical importance for space vehicles in defense industry. Among all of the radar absorption mechanisms, use of frequency selective surface has become prominent. In this thesis, composite material having frequency selective surface was developed, manufactured and characterized. Designing of frequency selective surface operating in 8.2 – 12.4 GHz frequency range was conducted by means of finite element analysis method. In addition to radar absorbing performance, it was aimed to attain a material that can be used in structural parts. Therefore, frequency selective surface design procedure was carried out considering processability and mechanical properties of composite material. Radar absorbing performance of developed composite material was illustrated by using NRL Arch free space method. Furthermore, mechanical, thermal and physical characterization tests were applied.

Keywords: Composite Materials having Frequency Selective Surface, Radar Absorbing Composites, Finite Element Analysis, NRL Arch Method

ÖZ

FREKANS SEÇİCİ YÜZEY İÇEREN KOMPOZİT MALZEMELERİN RADAR SÖNÜMLEME PERFORMANSLARININ NÜMERİK VE DENEYSEL İNCELENMESİ

Subaşı, Buse
Yüksek Lisans, Metalurji ve Malzeme Mühendisliği
Tez Yöneticisi: Doç.Dr. Caner Şimşir
Ortak Tez Yöneticisi: Doç.Dr. Bektaş Çolak

Kasım 2022, 90 sayfa

Savunma sanayiinde, uzay araçları için radar sönümleme özelliği gösteren malzemeler kritik bir öneme sahiptir. Son zamanlarda, tüm radar sönümleme mekanizmaları arasında frekans seçici yüzey kullanımı öne çıkmaktadır. Bu tezde, frekans seçici yüzey içeren kompozit malzeme geliştirilmiş, üretilmiş ve karakterize edilmiştir. 8.2 – 12.4 GHz frekans aralığında çalışan frekans seçici yüzey tasarımı sonlu eleman analiz yöntemiyle yapılmıştır. Radar sönümleme performansına ek olarak, yapısal parçalarda kullanılabilen malzeme elde edilmesi de amaçlanmıştır. Bu sebeple, frekans seçici yüzey tasarım süreci, proses edilebilirlik ve kompozit malzemenin mekanik özellikleri göz önünde bulundurularak yürütülmüştür. Geliştirilen kompozit malzemenin radar sönümle performansı NRL Arch serbest uzay yöntemiyle gösterilmiştir. Ayrıca, mekanik, termal ve fiziksel karakterizasyon testleri de uygulanmıştır.

Anahtar Kelimeler: Frekans Seçici Yüzey içeren Kompozit Malzemeler, Radar Sönümleyen Kompozitler, Sonlu Eleman Analizi, NRL Arch Metodu

To My Family

ACKNOWLEDGMENTS

I would like to express my deepest gratitude to my supervisor Assoc. Prof. Dr. Caner Şimşir and co-supervisor Assoc. Prof. Dr. Bektaş Çolak for their guidance, advice, criticism, encouragements and insight throughout the research.

I would like to express my sincere thanks to my family and my best friend Ezgi Akçay who support me from the beginning with their love and patience.

Finally, I would like to thank ROKETSAN A.Ş. for financial support.

TABLE OF CONTENTS

LIST OF TABLES

TABLES

LIST OF FIGURES

FIGURES

CHAPTER 1

INTRODUCTION

1.1 Preface

Radar systems (Radio Detection and Ranging Systems) are to detect the velocity and location of aerospace vehicles by use of radio waves. Electromagnetic waves within the frequency of radio frequency interval range are transmitted and collected back after reflection of the target, which is analyzed in order to acquire the knowledge about the target, such as location and velocity. The detectability of a substance by the radar systems is defined as the radar cross section. The equivalent area formed on the radar detector due to the reflected electromagnetic waves is the basis of radar cross section, which is influenced by geometrical shape and material properties of the body, frequency and the incident angle of the radar waves [1]. Radar absorbing composite materials are developed to decrease radar cross section area by means of absorbing the electromagnetic waves within a certain frequency range in order to reduce the reflection. There are different absorbing mechanisms and materials available for composite materials.

1.2 Particle Based Loss Mechanism

When an electromagnetic wave propagating in air meets with a new media having different intrinsic impedance than air, some portion of it is reflected while some portion is transmitted. Intrinsic impedance, η, is the amount of resistance shown by a medium to a propagating electromagnetic wave. It can be calculated by Equation 1.2.1 [2] where Z_0 is impedance of free space that is $377\ \Omega$.

$$\eta = \sqrt{\frac{\mu}{\varepsilon}} = \sqrt{\frac{\mu_0 \mu_r}{\varepsilon_0 \varepsilon_r}} = Z_0 \sqrt{\frac{\mu_r}{\varepsilon_r}} \quad (1.2.1)$$

Amount of lost energy due to reflection is defined as reflection loss (RL) and described by Equation 1.2.2, Equation 1.2.3 and Equation 1.2.4 in which Z_{in}, γ , λ and d are input impedance of media, propagation constant, wavelength of the electromagnetic wave and thickness of medium [3].

$$RL = 20 \log \left| \frac{Z_{in} - Z_0}{Z_{in} + Z_0} \right| \quad (1.2.2)$$

$$Z_{in} = \eta \tanh(\gamma d) \quad (1.2.3)$$

$$\gamma = j \frac{2\pi}{\lambda} \sqrt{\mu \varepsilon} \quad (1.2.4)$$

As it can be interpreted from Equation 1.2.2, if input impedance and impedance of free space is equal to each other, there is no reflection of electromagnetic wave from the surface. Therefore, as input impedance of surface of a material gets closer to 377 Ω , reflection of radio wave due to impedance mismatch is minimized. For the multiple layer absorber, Z_{in} can be calculated as given in Equation 1.2.5 [3].

$$Z_i = \eta_{i+1} \frac{\eta_{i-1} \tanh(\gamma_{i-1} d_{i-1}) + \eta_i \tanh(\gamma_i d_i)}{\eta_i + \eta_{i-1} \tanh(\gamma_{i-1} d_{i-1}) \tanh(\gamma_i d_i)} \quad (1.2.5)$$

Radar absorbing composite materials having particle based loss mechanism aim to design permittivity and permeability of composite layers so that impedance of composite material is suitable for effective electromagnetic absorption.

Nano/micro particles having dielectric and magnetic properties can be employed to attain particle based loss mechanism. In literature, carbonaceous materials such as carbon black, carbon nanotube, multi-walled carbon nanotube and carbon nanofibers as dielectric absorber, and iron-based particles such as carbonyl iron and ferrite were

widely used to study electromagnetic wave absorbing properties [4-9]. These particles can be dispersed into matrix material (epoxy, rubber etc.) or can be coated on fiber reinforcement element (glass fiber, carbon fiber etc.) of composite materials.

In addition to use of one type of absorber, both dielectric and magnetic particles can be applied in order to operate both loss mechanisms in the same structure. Also, to improve electromagnetic wave absorption properties, hybrid type particles such as Ag@CNT [10], Fe_3O_4@MWCNT [11], Ni_2P@CNT [12], SiC@SiO_2 [13] were synthesized and examined.

1.2.1 Dielectric Loss

Dielectric materials are non-conducting materials which contain negative and positive charges. When exposed to electric field, this positive and negative charges align towards the electric field direction. The process of alignment of the structures such as ion, dipole and electron cloud within dielectric material is called polarization [14].

Any material, which electric field is applied to, causes energy loss by converting some of the electric energy into heat. This energy loss for dielectric materials is called dielectric loss. Different from conducting materials, dielectric loss is directly related to frequency of applied alternative voltage [15]. Electric field that changes with frequency alternates the polarization direction by realigning ions, dipoles and electron clouds. The required time for displacement and direction change is called dielectric relaxation time. In the case that dielectric relaxation time and electromagnetic wave frequency are matched with each other, the electromagnetic wave coming to the material is converted into heat and absorbed [16].

Dielectric materials are characterized by dielectric permittivity properties. Dielectric permittivity consists of real and imaginary parts as shown in the Equation 1.2.6. It shows the material's ability to be polarized. Real part of relative permittivity (ε_r'), which was calculated by dividing dielectric permittivity of material to that of vacuum

($\varepsilon_0 = 8.854 \times 10^{-12}\ F/m$) , expresses the energy storage ability of the material while imaginary part of relative permittivity value (ε_r'') represents the energy distribution or loss capability [17].

$$\varepsilon = \varepsilon_0(\varepsilon_r' - \varepsilon_r'' j) \tag{1.2.6}$$

1.2.2 Magnetic Loss

Magnetic materials are polarized under magnetic field and therefore have an absorption mechanism which works similarly to dielectric materials [14]. According to their behavior under magnetic field, they are categorized as diamagnetic, paramagnetic, ferromagnetic, ferrimagnetic and anti-ferrimagnetic.

Materials under the time varying magnetic field result in magnetic loss, which is called core loss or iron loss. This loss is the sum of hysteresis loss and Eddy current losses [6]. Magnetic induction in a material which is under magnetic field (H) is called flux density. Ferromagnetic and ferrimagnetic materials can stay magnetized even if applied magnetic field is removed and their magnetic polarization directions can change when magnetic field direction is altered. This is called hysteresis loop. In each loop, there is an energy loss named as hysteresis loss due to delay of reaction in the material against applied magnetic field [18]. Hysteresis loss is directly proportional to hysteresis cycle curve, which is specific to each material. Eddy current loss is originated from materials' conductive natures. When ferromagnetic materials are exposed to magnetic field which changes according to a certain frequency, the electromagnetic force formed inside the material causes a current which is called Eddy current. Eddy current opposes the changes in the magnetic field and alters direction accordingly, which gives rise to energy loss because of the resistance it applies [19]. Similar to dielectric materials, magnetic materials are characterized by permeability constant, given in Equation 1.2.7, which is represented by real and imaginary parts of relative permeability that is the ratio of permeability of material and permeability of free space ($\mu_0 = 4\pi \times 10^{-7}\ Henry/m$).

$$\mu = \mu_0(\mu_r' - \mu_r'' j) \quad (1.2.7)$$

1.3 Resonant Type Loss Mechanism

Resonant type of mechanism makes use of annihilation of reflected waves due to the phase difference between electromagnetic waves. In order to accomplish resonant loss, resistive sheet, spacer and perfect electric conductor layer are used in this type mechanism. Salisbury screen, Dallenbach layer and Jaumann layer absorbers are the elemental designs of resonant type loss mechanism while Circuit analog absorbers are more recent studies in radar absorbing material research area.

1.3.1 Salisbury Screen

Salisbury screen absorber consists of a perfect electric conductor layer such as a metal plate and a resistive sheet that is placed at a distance of $\lambda/4$ from the metal plate. In between the metal plate and resistive sheet, there is a lossless dielectric material, called spacer [20]. The resistive sheet generally has $377\ \Omega$ input impedance in order to provide impedance matching with the free space. The schematic shown of a Salisbury screen absorber is given in Figure 1.1. When an electromagnetic wave meets with the resistive sheet, some portion of it is reflected and the rest is transmitted to the spacer material and reaches to perfect electric conductor. Then, it is reflected back towards the resistive sheet. Due to the specific distance of $\lambda/4$, there occurs $\lambda/2$ $(\lambda/4 + \lambda/4)$ delay between these waves. When the wave reflected by perfect electric conductor reach to and interfere with the wave reflected by resistive sheet, because of $\lambda/2$ phase difference, they cancel each other. This results in complete cancelation of reflection. [21].

Since only electromagnetic wave with a wavelength specific to separation distance of resistive sheet and metal plate can be absorbed, Salisbury screen is a narrowband absorber, restricted to certain resonant frequency [22].

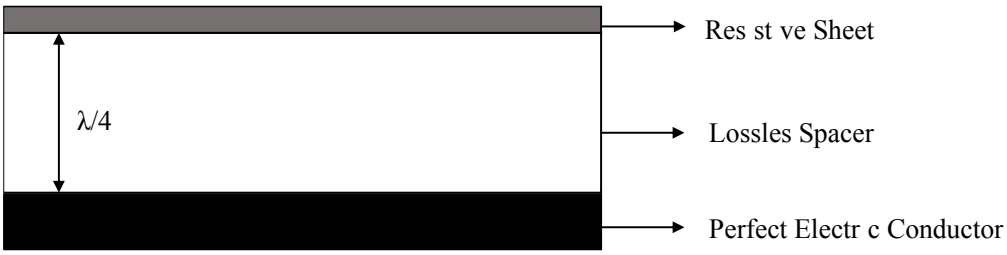

Figure 1.1 Schematic Shown of Salisbury Screen structure

1.3.2 Dallenbach Layer

Dallenbach layer is a resonant type of absorber that contains perfect electric conductor and lossy medium (Figure 1.2). In this absorber design, surface impedance should be matched with the free space impedance in order not to have reflection of incident wave from the surface. The propagation wave is absorbed within the lossy media which have dielectric permittivity (ε) and/or magnetic permeability (μ) properties [23]. Thickness of the lossy medium can be tuned so that absorption can take place in desired frequency of wave by means of destructive interference. To provide broadband absorption, rather than single layer, multiple layers of absorbers can be placed [24]. While designing of such Dallenbach layer absorber, dielectric and magnetic properties and thickness of each layer should be arranged such that there forms a gradient impedance within the structure and reflection of wave is minimized.

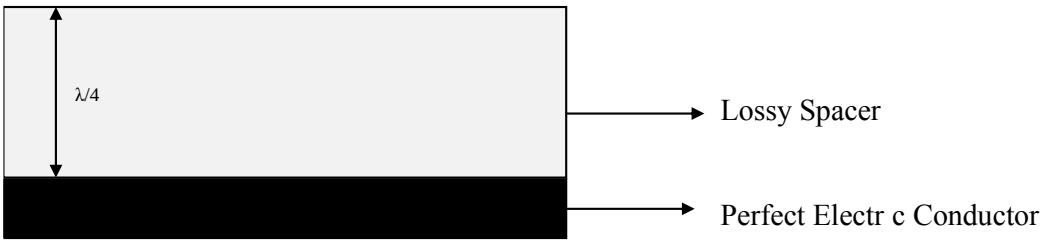

Figure 1.2 Schematic shown of Dallenbach Layer

1.3.3 Jaumann Layer

Jaumann layer type of absorbers can be identified as a version of Salisbury screen with more than one resistive sheet (Figure 1.3). As the number of resistive sheets is increased, the variability of frequency of absorbed waves can be increased [25]. Also, positioning the resistive sheets is done in decreasing order of resistivity of the sheets from surface towards the perfect electric conductor [26]. However, increase in thickness and weight of the material can limit the use of Jaumann layer type of structures.

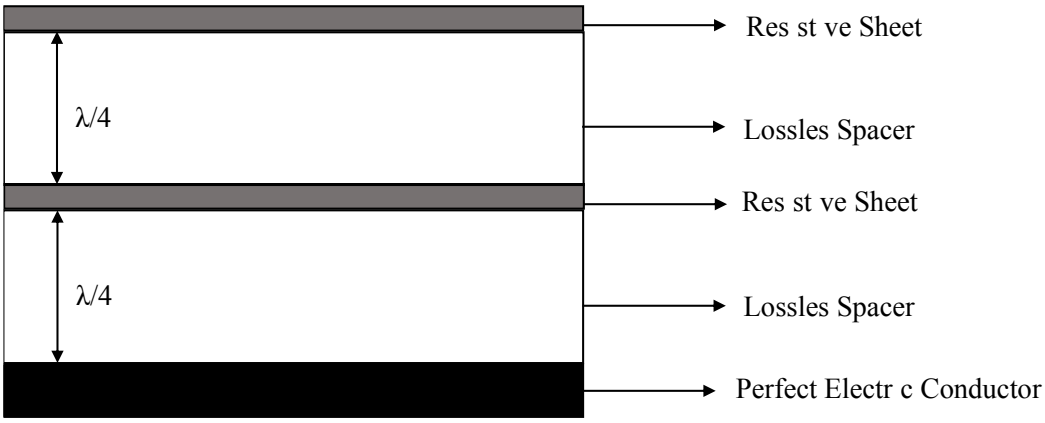

Figure 1.3 Schematic shown of Jaumann Layer

1.3.4 Circuit Analog Absorbers

Circuit analog absorbers consist of frequency selective surfaces which are periodically designed systems having conductive patches or apertures and they are aimed to reflect or transmit electromagnetic waves with certain frequencies. Setting the resonance frequency value by playing with shape, size and period of conducting elements that are placed on dielectric surface, transmission or blocking of desired electromagnetic wave can be provided [27].

Unit cell of frequency selective surface determines the characteristic of circuit analog absorbers. In terms of their reaction to the incident electromagnetic wave, unit cells can be sorted as high-pass, low-pass, band-stop or band-pass type [28]. Behavior of unit cell types is shown in Figure 1.4. Low-pass structures are composed of conducting patches on their surface and they allow electromagnetic waves having frequency lower than cutoff frequency to pass. Oppositely, high-pass structures contain apertures on conducting surface and transmit higher frequencies than cutoff frequency. Band-stop unit cells are designed to prevent certain range of frequency to pass through the structure, while band-pass unit cells transmit only a specific range of frequency.

As stated in previously, impedance of the FSS effects the reflection loss of the radar absorber structure. The impedance of FSS layer can be calculated analytically by using transmission line theory and equivalent circuit model.

An electromagnetic wave causes inductive and capacitive effects on the frequency selective surface. For instance, when an electromagnetic wave, shown in Figure 1.5, is exposed to FSS structure with square patches, there occurs an electric field through the vertical gap of unit cells, which causes the square patches to represent capacitive behavior. Similarly, magnetic field of incident electromagnetic wave creates a current in the vertical strips which results in secondary magnetic field around the vertical strips. Due to that, FSS has an inductive behavior [29].

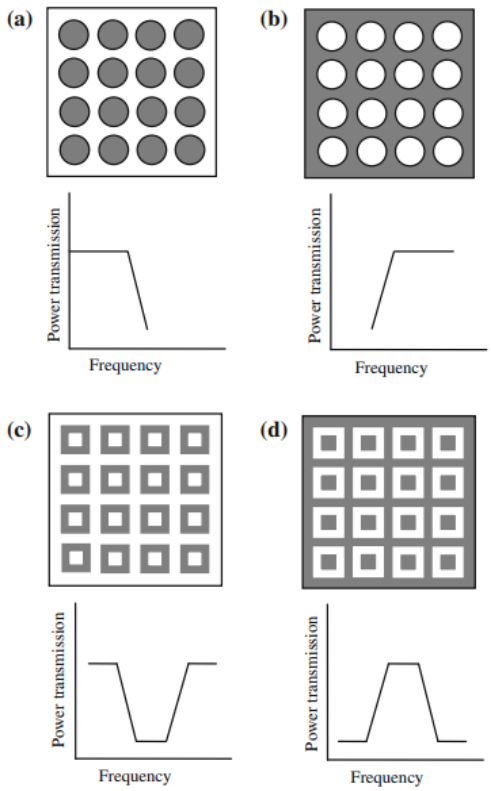

Figure 1.4 Reaction of unit cells having a)low-pass characteristics, b)high-pass characteristics, c)band-stop characteristics and d)bans-pass characteristics [28]

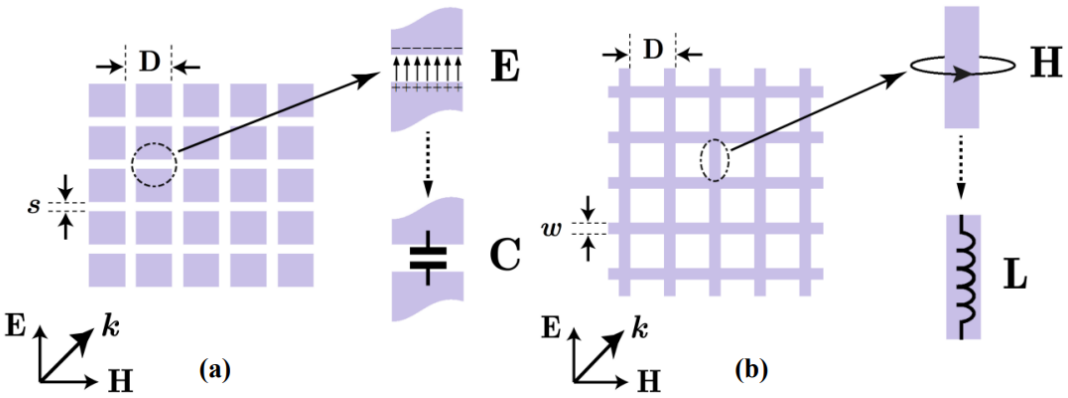

Figure 1.5 The geometric configuration of square patch array. This array acts as a capacitor exposed by a TEM incident wave with the shown polarization. (b) The geometric configuration of square strip array. This array acts as an inductor exposed by a TEM incident wave with the shown polarization [29]

Impedance of a frequency selective surface is given in Equation 1.3.1 where R is the resistance, and X is the reactance of frequency selective surface. Schematic shown of equivalent circuit model of a circuit analog absorber consisting of square patch-based frequency selective surface and a dielectric substrate can be seen in Figure 1.6.

$$Z_{FSS} = R - Xj \tag{1.3.1}$$

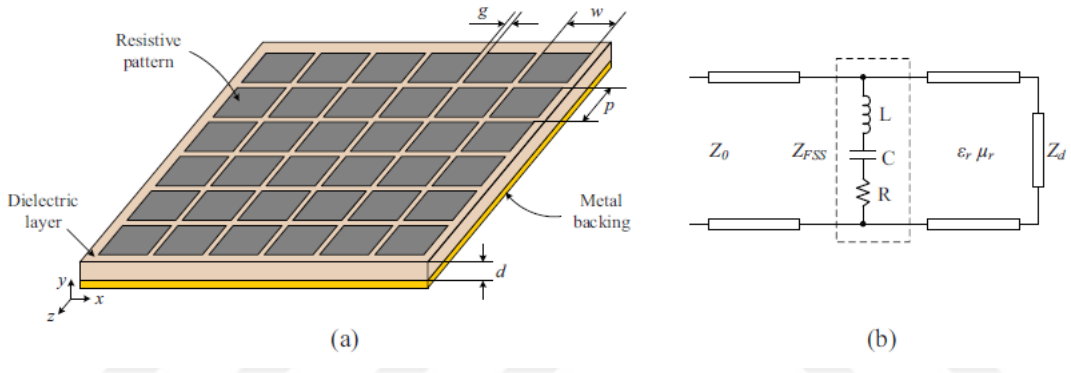

Figure 1.6 a) Geometry of square patch FSS and b) equivalent circuit model [30]

Equivalent resistance of the FSS is given in [31] by Equation 1.3.2 in which R is resistance of FSS, R_s is surface resistance, S is area of unit cell and A is effective surface area of unit cell. For a square patch unit cell, S is p^2 and A is d^2 where p is periodicity and d is size of the square patch.

$$R = R_s \frac{S}{A} \tag{1.3.2}$$

Reactance of frequency selective surface can be calculated using equivalent circuit model by using inductance (L) and capacitance (C) parameters.

Normalized inductive reactance (X_L) and capacitive susceptance (B_c) can be calculated by using Equation 1.3.3 through Equation 1.3.8 given by Marcuvitz in [32] where Z_0 is impedance of free space, p is the periodicity of unit cell, θ is the incidence angle and λ is the wavelength of electromagnetic wave, w is the thickness of the inductive strip, g is the gap between the unit cell and G is the correction factor.

$$\frac{X_L}{Z_0} = \frac{p\cos\theta}{\lambda}\left[\ln\left(cosec\left(\frac{\pi w}{2p}\right)\right) + G\right] \tag{1.3.3}$$

$$\frac{B_C}{Y_0} = \frac{4\,p\cos\theta}{\lambda}\left[\ln\left(cosec\left(\frac{\pi g}{2p}\right)\right) + G\right] \tag{1.3.4}$$

$$G = \frac{1}{2}\frac{(1-\beta^2)^2\left[\left(1-\frac{\beta^2}{4}\right)(A_1+A_2) + 4\beta^2 A_1 A_2\right]}{\left(1-\frac{\beta^2}{4}\right) + \beta^2\left(1+\frac{\beta^2}{2}-\frac{\beta^4}{8}\right)(A_1+A_2) + 2\beta^6 A_1 A_2} \tag{1.3.5}$$

$$A_{1,2} = \frac{1}{\sqrt{1 \pm \frac{2p\,sin\theta}{\lambda} - \left(\frac{p\,cos\theta}{\lambda}\right)^2}} - 1 \tag{1.3.6}$$

$$\beta = \sin\left(\frac{\pi w}{2p}\right), for\ inductive\ strips \tag{1.3.7}$$

$$\beta = \sin\left(\frac{\pi g}{2p}\right), for\ capacitive\ strips \tag{1.3.8}$$

After calculating inductive reactance (X_L) and capacitive susceptance (B_C,), unit cell design parameters of inductance (L) and capacitance (C) can be determined using Equation 1.3.9, Equation 1.3.10 and Equation 1.3.11 where ω is the angular frequency of incident electromagnetic wave [33].

$$X_L = \omega L \tag{1.3.9}$$

$$X_C = \frac{1}{B_C} = \frac{1}{\omega C} \tag{1.3.10}$$

$$\omega = 2\pi f \tag{1.3.11}$$

Resonance frequency of a FSS layer is very important characteristic of a radar absorbing structure and it is achieved when reactance of FSS is zero [34]. Considering a FSS having both inductive and capacitive feature, resonance frequency, f_R, can be calculated Equation 1.3.12.

$$f_R = \frac{1}{2\pi\sqrt{LC}} \tag{1.3.12}$$

Design of a circuit analog absorber structure can be done with both analytical calculations and numerical analysis. A radar absorber structure can be represented by equivalent circuit model as shown in Figure 1.7b. Since FSS1 and Spacer1 are connected parallel to each other, input impedance at point A can be evaluated as in Equation 1.3.13.

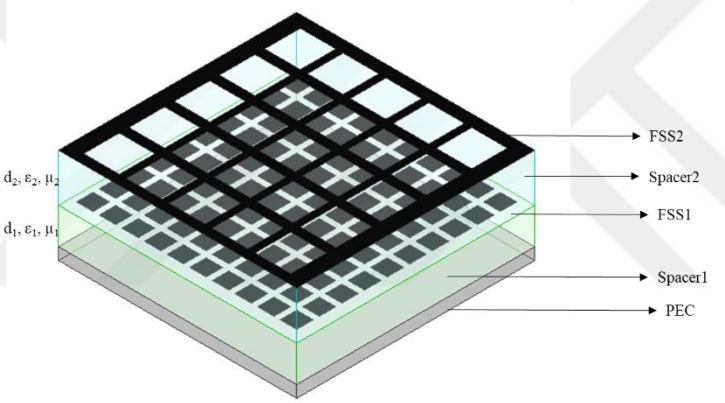

(a)

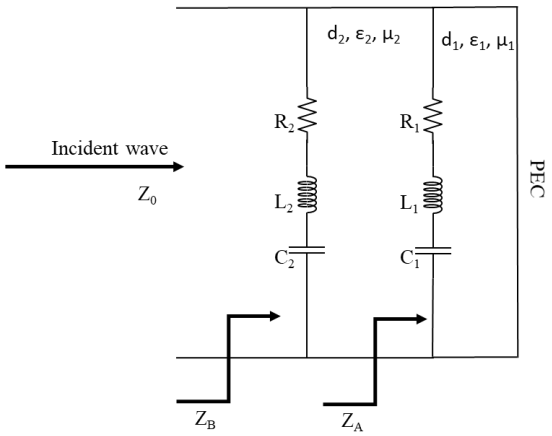

(b)

Figure 1.7 Illustration of a) a circuit analog absorber structure, b) equivalent circuit model

$$Z_{FSS1} \parallel Z_{Spacer1}$$

$$\frac{1}{Z_A} = \frac{1}{Z_{FSS1}} + \frac{1}{Z_{Spacer1}} \tag{1.3.13}$$

Then, importing Equation 1.2.3 and Equation 1.3.1, Equation 1.3.9 and Equation 1.3.10 into Equation 1.3.13 results in

$$\frac{1}{Z_A} = \frac{1}{R_{FSS1} + j\left(\omega L + {}^{1}/_{\omega C}\right)_{FSS1}} + \frac{1}{\sqrt{\frac{\mu_{Spacer1}}{\varepsilon_{Spacer1}}}\tanh\left(\gamma_{Spacer1} d_{Spacer1}\right)} \tag{1.3.14}$$

Input impedance at point B is established using Equation 1.2.5 since it should be considered as multilayer structure.

$$\frac{1}{Z_B} = \frac{1}{R_{FSS2} + j\left(\omega L + {}^{1}/_{\omega C}\right)_{FSS2}} + \frac{1}{Z_{Spacer2}\dfrac{Z_A + \sqrt{{}^{\mu_{Spacer2}}/_{\varepsilon_{Spacer2}}}\tanh\left(\gamma_{Spacer2} d_{spacer2}\right)}{\sqrt{{}^{\mu_{Spacer2}}/_{\varepsilon_{Spacer2}}} + Z_A \tanh\left(\gamma_{Spacer2} d_{spacer2}\right)}} \tag{1.3.15}$$

Reflection loss of this structure would be

$$RL = 20 \log \left| \frac{Z_B - Z_0}{Z_B + Z_0} \right|. \tag{1.3.16}$$

Parameters of FSS, which are inductance, capacitance and resistance are already discussed above. For inductance and capacitance properties, size and shape of unit cell are controlled. For resistance property, both unit cell size and shape and also surface resistivity of used material are important (see Equation 1.3.2). In literature, use of both perfect electric conducting material (metallic elements) and resistive materials (conductive inks) can be seen.

As it can be seen in Equation 1.3.15, reflection loss of a circuit analog absorber depends on not only frequency selective surface parameters (resistance, inductance and capacitance), but also properties of spacer material (thickness, dielectric permittivity and magnetic permeability of spacer), therefore spacer material and its thickness play an important role on response of the radar absorber structure to the incident electromagnetic wave. In literature, it is seen that mostly two different kind of spacer material are selected based on design strategy. The first kind is foam material since its dielectric permittivity is very close to that of air such that it does not interfere with propagation of electromagnetic wave through the thickness of spacer. The other mostly used spacer material is FR4 plate, which is a commercially available glass fiber reinforced epoxy matrix composite plate having well defined homogeneous dielectric properties. Also, FR4 plate is a good substrate for printing FSS, which eliminates the need of substrate material. Combination of both spacer material in a radar absorber structure can also be applied [35].

In order to have a proper design, meeting the requirements, optimization of radar absorber structure is necessary. To do so, genetic algorithm (GA) with computation tools such as MATLAB together with finite element simulation tools such as Ansys HFSS and CST Studio are mostly used in literature. In [36], a double layer circular loop unit cell (Figure 1.8) is proposed and transmission loss behavior is determined and optimized with both equivalent circuit model and finite element simulation using CST. As shown in Figure 1.9, they are in good agreement with transmission behavior result. In this work, FSS is produced by photo-lithography technique and a very thin (0.127 mm) FR4 plate is used as spacer material. Similarly, in [38], a square patch FSS is manufactured by silk printing method and 3.2 mm thick ROGERS\RO4003 spacer is used. Equivalent circuit model with the help of MATLAB and also Ansys HFSS simulation tool are employed for optimization of unit cell size for desired reflection behavior.

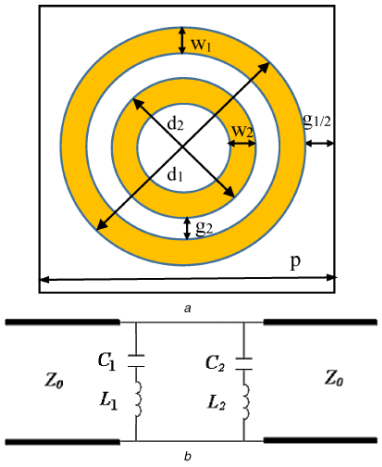

Figure 1.8 a) Double layer circular loop unit cell and b) equivalent circuit model [36]

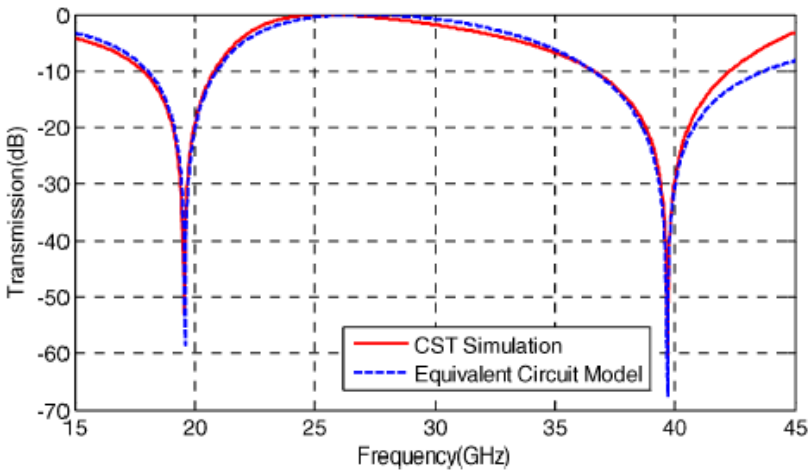

Figure 1.9 Equivalent circuit model and finite element simulation results for double layer circular loop structure [36]

1.4 Objective of the Thesis

Looking in literature, it can be realized that most of the works related with FSS focus on reflection/transmission behavior regardless of mechanical/physical/thermal property of the structure. Use of FR4 plate, dielectric material or foam material as spacer material facilitates both the design and process of absorber structure. They may be convenient for some reflector/transmitter systems such as antennas. However, for a structural composite part, they are not suitable to be used in terms of processability and mechanical/physical/thermal properties. For instance, using commercially available flat FR4 plate cannot be shaped for desired geometry. Foam materials are hard to be shaped and their mechanical as well as durability to environmental conditions may be insufficient. Also, using foam material requires an adhesive layer for FSS to be consolidated. Adhesive layers are mostly inadvisable since they have great potential for delamination or crack initiation. This risk gets even higher for structures having more than one FSS layer. Therefore, a spacer material that can be shaped to a desired geometry and used as structural member together with appropriate electromagnetic properties (ε_r, μ_r) is required to produce composite radar absorber part.

Not only spacer material but also top surface which is open to air should be taken in consideration. For example, leaving FSS layer open to the air might result in problems such as peeling or degradation. Therefore, a layer covering the FSS layer is essential.

Finally, placing a perfect electric conductor layer is important to construct ground plane. To do so, mostly copper panel is used in literature, which is attached to the structure with adhesive agent. For a structural composite, that might generate peeling problem.

The objective of this thesis is to design a radar absorber composite material in a material engineer's point of view, which considers not only reflection/transmission

behavior but also processability and mechanical/physical/thermal performance of the material. In order to achieve this goal,

- finite element analysis was carried out to design composite material having FSS absorber working in X band (8.2 – 12.4 GHz) using Ansys HFSS tool,
- composite plate was produced for experimental verification
    - FSS layer was manufactured with screen printing method
    - prepreg lay-up production technique was chosen since it allows to give desired geometry
    - glass fiber reinforced prepreg material is used as spacer material and carbon fiber reinforced prepreg material is used as perfect electric conductor layer
- reflection loss behavior was measured using NRL Arch method
- mechanical, physical and thermal characterization tests were done so that effect of using FSS layer in composite material can be evaluated.

CHAPTER 2

DESIGN OF COMPOSITE MATERIAL WITH FREQUENCY SELECTIVE SURFACE

In this work, Ansys HFSS tool was used to desigh the composite material with FSS layer. Design procedure included the steps given below:

1. Determining design parameters
2. Defining limitations of parameters
3. Characterization of fixed parameters
4. Designin composite material with FSS by means of numerical analysis

2.1 Determining Design Parameters

Representative image of composite material and its components are shown in Figure 2.1

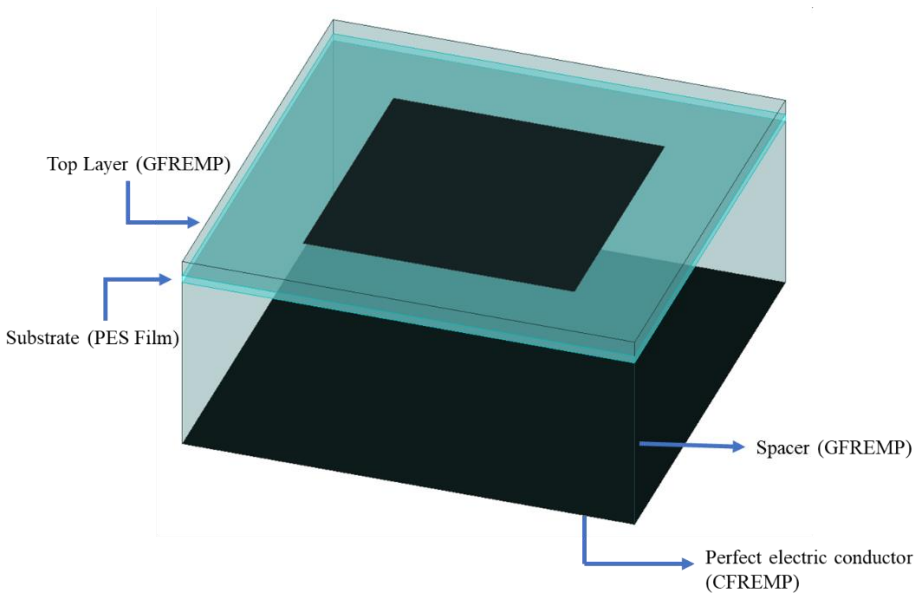

Figure 2.1 Components of composite material designed in this study

Design parameters for a composite material having FSS layer are listed below.

A. Electromagnetic properties (dielectric permittivity and magnetic permeability) of spacer material
B. Thickness of spacer material
C. Electromagnetic properties (dielectric permittivity and magnetic permeability) of substrate material of FSS layer
D. Thickness of substrate material
E. Unit cell design (shape, periodicity and size) of FSS layer
F. Surface resistance of conductive ink
G. Electromagnetic properties (dielectric permittivity and magnetic permeability) of top layer material
H. Thickness of top layer

2.2 Defining Limitations of Parameters

In order to form both the spacer material and top layer, glass fiber reinforced epoxy matrix prepreg (GFREMP) material was used. A prepreg material which is frequently used for structural composite part productions was chosen to construct composite material in this work. Since prepreg material was determined, spacer material's and top layer's electromagnetric properties can be considered as fixed design parameters. As substrate material, 125 μm thick PES film, which is commonly used in screen printing process, was selected. Since it is a shelf product, substrate material's electromagnetic properties and also thickness are also fixed design properties. Finally, a commercially available conductive ink for screen printing process was decided to be used to form unit cell of FSS. Hence, surface resistance of conductive ink is another fixed design property. Details about the used materials (prepreg, PES film and conducitve ink) are given in upcoming chapters.

As a result, thickness of spacer material, unit cell design and thickness of top layer are the design variables in this work.

2.3 Characterization of Fixed Parameters

Prior to numerical analysis, characterizations of fixed parameters were performed so that values of input parameters can be determined. Details about experimental procedure and also test results are given in upcoming chapters. Properties of design parameters can be found in Table 2.1. In addition to average values, minimum and maximum values of test results are also given in Table 2.1. It should be noted that since the spacer material was manufactured by prepreg lay-up process, thickness of spacer and top layer were determined by the thickness of single GFREMP layer, which is called as ply thickness. Therefore, number of GFREMP layer together with the ply thickness were considered as design parameters for spacer and also top layer material.

Table 2.1 Values of design parameters

Design Parameters	Average Value	Minimum and Maximum Values of Measurement Results
Electromagnetic properties of spacer material	$\varepsilon_r = 3.9768$ $\tan\delta = 0.0049$	$\varepsilon_r = 3.9239$, $\tan\delta = 0.0067$* $\varepsilon_r = 4.02975$, $\tan\delta = 0.0032$
Electromagnetic properties of substrate material	$\varepsilon_r = 3.2$ $\tan\delta = 0.003$	-
Thickness of substrate material	0.128 mm	Minimum: 0.124 mm Maximum: 0.131 mm
Surface resistance of conductive ink	75.1 Ω/sq	Minimum: 66.8 Ω/sq Maximum: 83.3 Ω/sq
Electromagntic properties of top layer material	$\varepsilon_r = 3.9768$ $\tan\delta = 0.0049$	$\varepsilon_r = 3.9239$, $\tan\delta = 0.0067$* $\varepsilon_r = 4.02975$, $\tan\delta = 0.0032$
Ply thickness	0.261 mm	Minimum: 0.255 mm Maximum: 0.267 mm
Thickness of spacer material	Design variable	
Unit cell design (shape, periodicity and size)	Design variable	
Thickness of top layer	Design variable	

*They are the results of two different measurements, not the minimum and maximum values

2.4 Designing Composite Material with Frequency Selective Surface

Desgining was conducted by means of numerical analysis using Ansys HFSS tool. Square patch unit cell type (Figure 2.2) was chosen in this study since it is widely studied in literature. However, as stated earlier, different than most of the works in literature, the entire composite material system including GFREMP and FSS unit cell was analysed in this work.

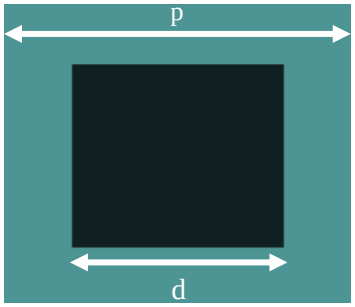

Figure 2.2 Square patch unit cell where d: unit cell size and p: periodicity

As a start, p=6 mm, d=4 mm for square patch unit cell was chosen and transmission behaviour of this unit cell structure was analyzed. In order to form periodically repeated square patch unit cell structure, master and slave boundaries were assigned (Figure 2.3). Floquet port was placed on top and bottom of the vacuum region for electromagnetic wave excitation (Figure 2.4).

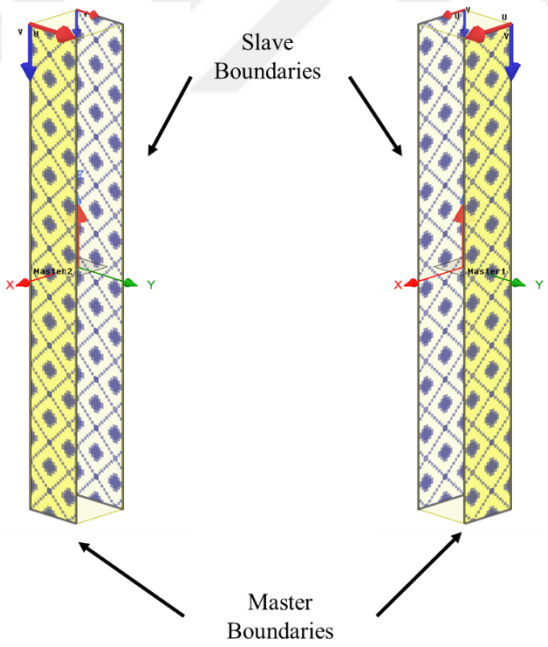

Figure 2.3 Master and slave boundaries applied to form periodically patterned unit cell structure

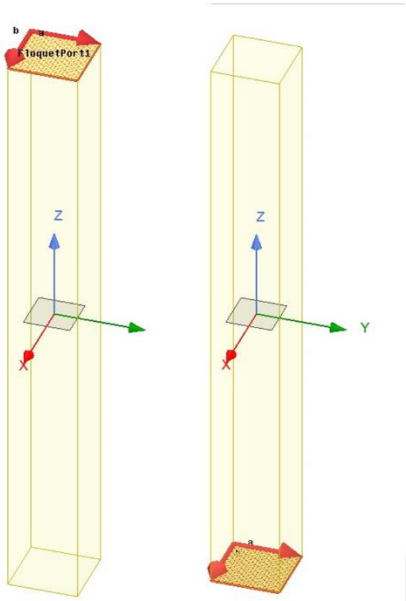

Figure 2.4 Floquet port excitation to determine reflection loss behavior

As shown in Figure 2.5, this square patch unit cell structure has a resonance frequency at 46.2 GHz ($\lambda = 6.48\ mm$). Since, the spacing between resistive element and perfect electrical conductor layer is arrenged as $\lambda/4$ in order to construct radar absorbing property, thickness of that structure was organized as 1.62 mm.

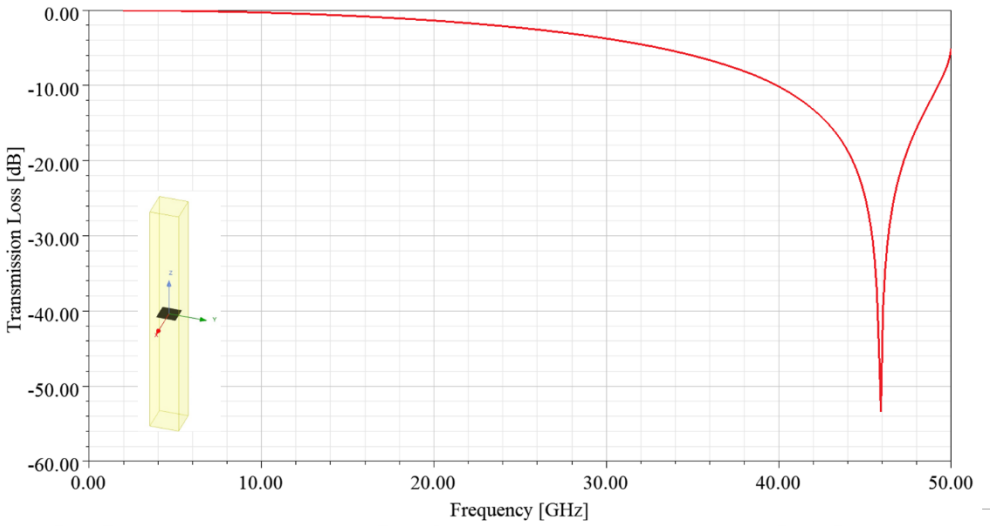

Figure 2.5 Transmission behavior of square patch unit cell (p=6mm, d=4 mm) in free space

After determinig the spacer thickness as 1.62 mm, reflection loss response of resistive square path was analysed. At that stage, impedance boundary condition was used to designate 75.1 Ω/sq surface resistance to the resistive square patch element (Figure 2.6). And also, at the bottom of the structure, an infinite ground plane having perfect electrical conductor boundary condition was inserted. This layer was to simulate CFREMP layers of the composite material (Figure 2.6). Resistive square patch (p=6 mm, d=4 mm) standing on 1.62 mm thick air spacer showed resonance frequency at 25.4 GHz, as shown in Figure 2.7.

Figure 2.6 (a) Impendance boundary for square patch unit cell and (b) perfect electric conductor boundary condition for CFREMP

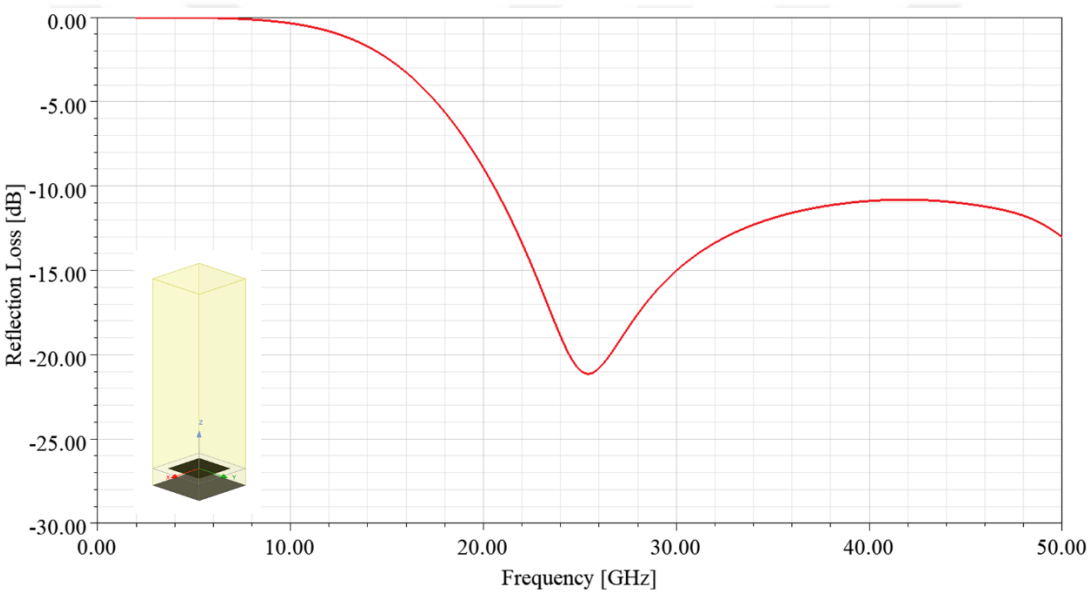

Figure 2.7 Reflection loss behavior of resistive square patch (p=6 mm, d= 4mm) standing on 1.62 mm thick air spacer

As a next stage, GFREMP spacer material was introduced in the place of air spacer. GFREMP, which was to form spacer and top layer material, was defined with dielectric properties of $\varepsilon_r = 3.9768$ and $\tan\delta = 0.0049$ (Figure 2.9). It is known that for the same thickness, a spacer material having dielectric permittivity (ε_r) greater than that of air ($\varepsilon = 1$) shifts the resonance frequency to the lower values with a relation defined by Equation 2.1.1 [27]. That means, replacing air with

GFREMP material would alter resonance frequency from 25.4 GHz to 16.1 GHz. Finite element analysis showed that resonance frequency shifted to 15.4 GHz, which is consistent with analytical calculations.

$$f_r = \frac{f_0}{\sqrt{(\varepsilon_r + 1)/2}} \tag{2.1.1}$$

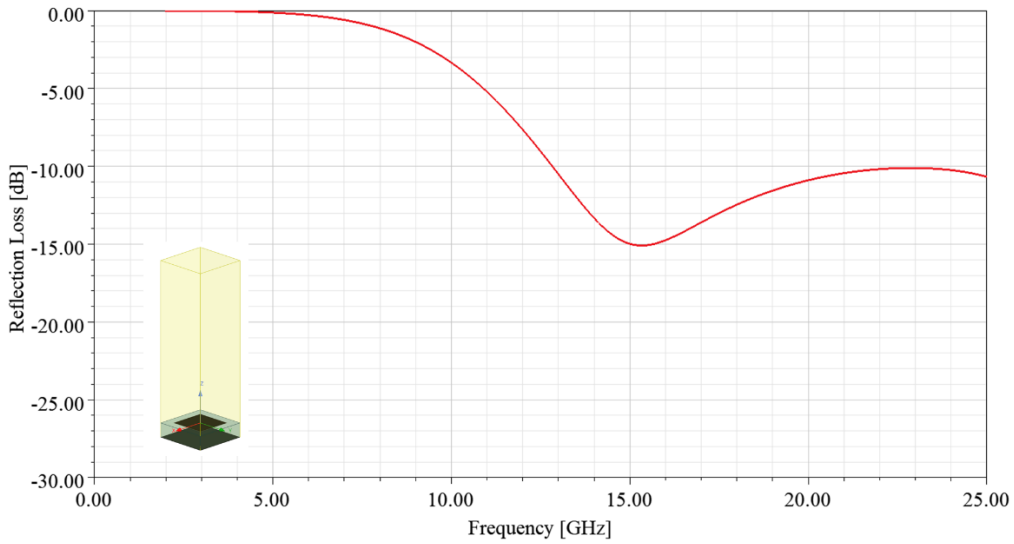

Figure 2.8 Reflection loss behavior of resistive square patch (p=6 mm, d=4 mm) standing on 1.62 mm thick GFREMP spacer

Since in this work FSS layer was formed on PES film, a substrate material, having 0.128 mm thickness, was located on the 1.62 mm thick GFREMP spacer. To form PES film substrate, material having dielectric properties of $\varepsilon_r = 3.2$ and $\tan\delta = 0.003$ was defined (Figure 2.9). As shown in Figure 2.10, this structure has a resonance frequency at 14.6 GHz. Thus, placing 0.128 mm thick PES film did not change reflection loss behavior of the structure significantly.

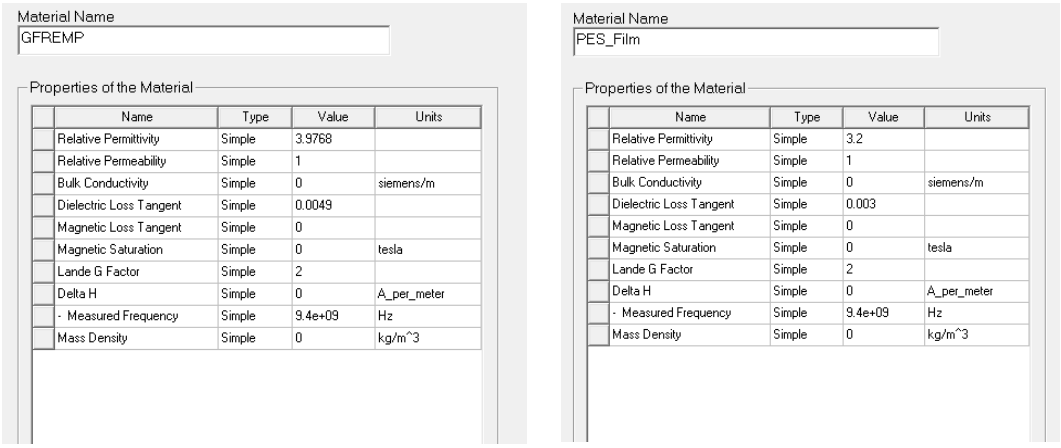

(a) (b)

Figure 2.9 Properties of (a) GFREMP to form spacer and top layer and (b) PES Film material to construct substrate

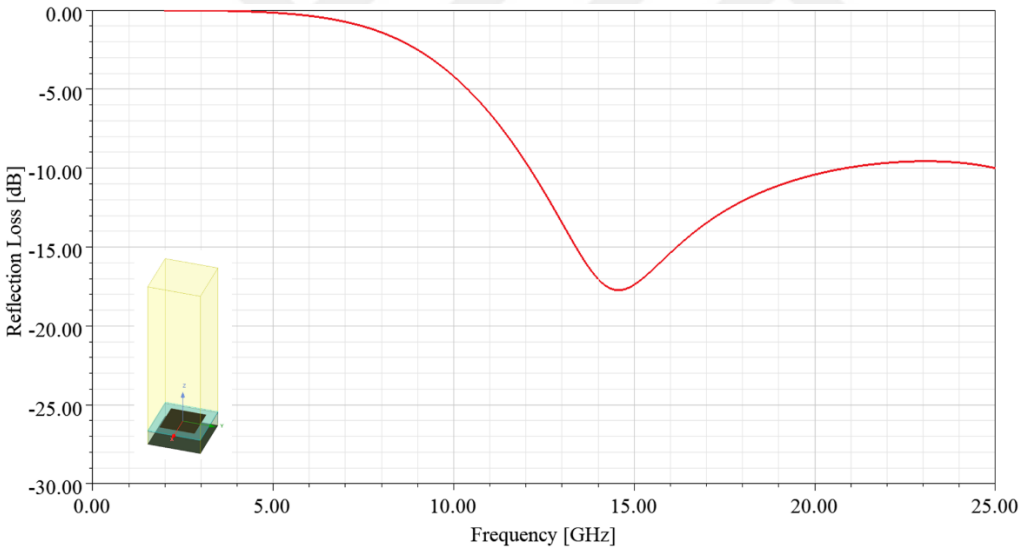

Figure 2.10 Reflection loss behavior of resistive square patch (p=6 mm, d=4 mm) having 0.128 mm PES film substrate and 1.62 mm thick GFREMP spacer

Effect of top layer material was shown in Figure 2.11. Increase in number of top layer from 0 to 2 decreases resonance frequency and S11 parameters. However, as explained before, covering the top of FSS layer is essential to protect material from

environmental impact. Therefore, rather than removing top layer form the structure, L_{top} =1 was selected as a limit for thickness of top layer material.

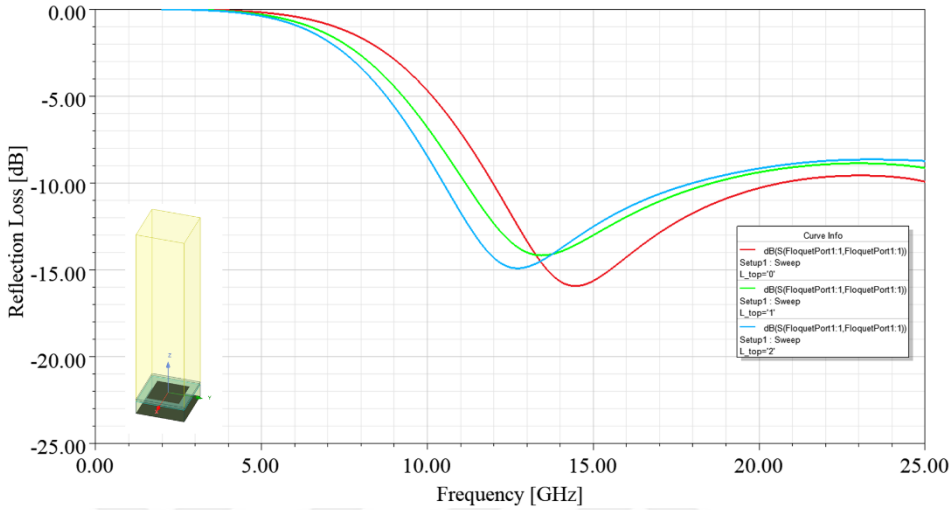

Figure 2.11 Reflection loss behavior of resistive square patch (p=6 mm, d=4 mm) having 0.128 mm PES film substrate and 1.62 mm thick GFREMP spacer and having different layer of top material

Since the purpose of this study is to design a composite material with FSS layer having radar absorbing property on X band frequency (8.2 – 12.4 GHz), design properties was optimized using "optimetric" tool in Ansys HFSS. Processability was taken into consideration while optimization was conducted. Since composite material was manufacured by means of prepreg lay-up, thickness of spacer was designated as $L_{spc} \times 0.261$ in which L_{spc} is the number of GFREMP layer used to form spacer and 0.261 is the cured ply thickness in mm. Simirlarly, thickness of top layer was defined as $L_{top} \times 0.261$ in which L_{top} is the number of GFREMP layer used to form top layer. Lower and upper limits of parameters in parametric setup are given in Table 2.1.

Table 2.2 Lower and upper limits of parameters defined in parametric setup

Parameter	Lower and Upper Values
Periodicity (p)	5 mm – 8 mm Step: 0.5mm
Unit cell size (d)	3 mm – 5 mm Step: 0.5 mm
Number of layer of GFREMP to form spacer (L_{spc})	6 – 12 layer Step: 1

Parametric analysis concluded that p=7.5 mm, d=4.5 mm, L_{spc}=10 (spacer thickness: 2.61 mm) would give 90% radar absorption property between in 8.2 GHz – and 13.2 GHz (Figure 2.12).

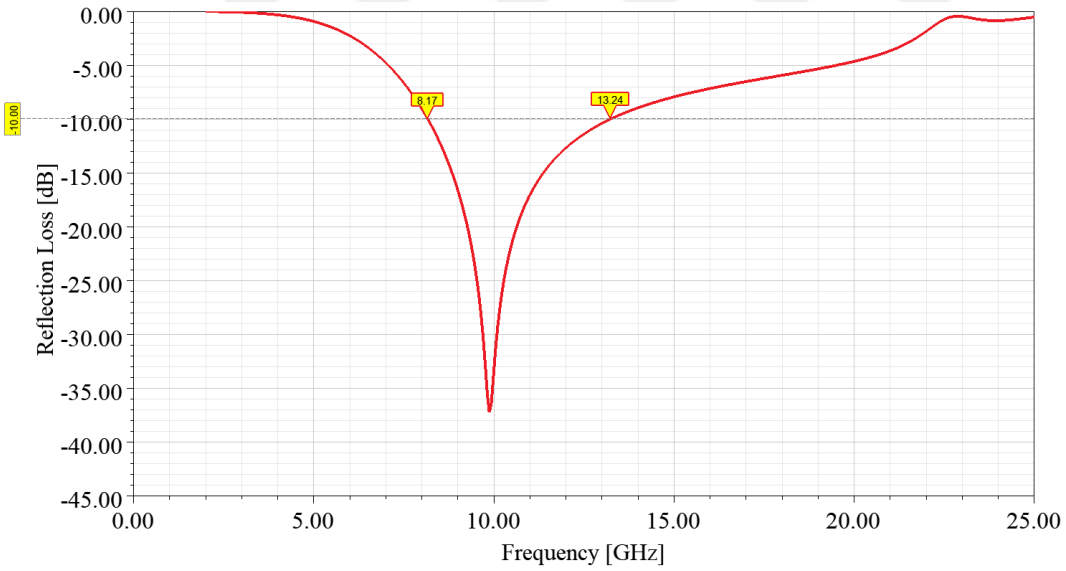

Figure 2.12 Finite element analysis of reflection loss behavior of designed composite material (p=7.5 mm, d=4.5 mm, spacer=2.61 mm, top layer=0.261 mm)

2.5 Sensitivity Analysis

Finite element analysis procedure was conducted by using average measurement values of design parameters (dielectric permittivy of GFREMP, surface resistance of conductive ink and ply thickness) as input parameters. However, as it can be seen in Table 2.1, results of measurements scattered within a certain range, which can cause deviation between finite element analysis and experimental test results. As the name implies, sensitivity analysis is a method to determine how sensivite is the ouput to the change in input parameters. In order to determine the effect of scattering in input design parameters' values, sensitivty analysis was conducted.

2.5.1 Sensitivty Analysis for Thickness of Substrate Material

Results of sensitivity analysis for substrate thickness are given in Figure 2.13 and Table 2.3. As it can be seen, change in substrate thickness did not change resonance frequency. Therefore, it can be said that resonance frequency does not sensitive to the change in substrate thickness from 0.125 mm and 0.131 mm. Reflection loss at resonance frequency altered between -32 dB and -38 dB. Although there was not a linear relation between substrate thickness and reflection loss, linear behavior was assumed and dimensionless sensitivity was calculated as 201% (see Table 2.3). That means 0.001 mm increase in substrate thickness leads to 0.201% decrease in reflection loss of the composite material. Therefore, it can be concluded that substrate thickness variation between 0.125 mm and 0.131 mm does not have a significant effect on reflection behavior of composite material.

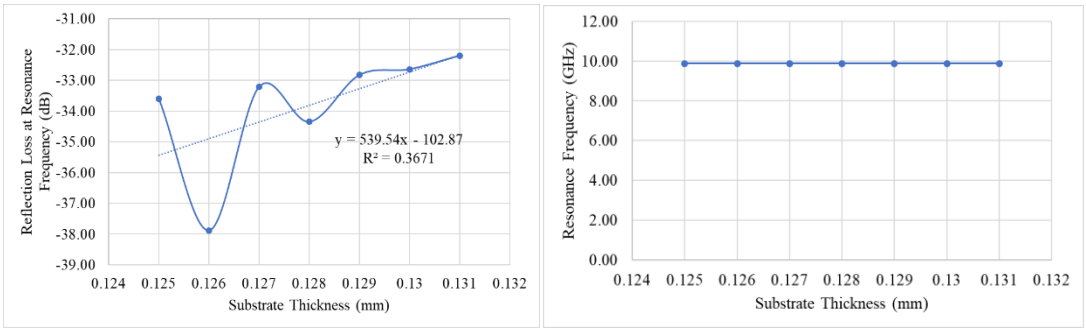

(a) (b)

Figure 2.13 Graphs of sensitivity analysis to determine effect of substrate thickness on (a) reflection loss at resonance frequency, (b) resonance frequency

Table 2.3 Results of sensitivity analysis for substrate thickness

Substrate Thickness (mm)	**Reflection Loss at Resonance Frequency (dB)**	**Resonance Frequency (GHz)**
0.125 (minimum measured)	-33.61	9.88
0.126	-37.88	9.88
0.127	-33.21	9.88
0.128 (nominal)	-34.34	9.88
0.129	-32.82	9.88
0.130	-32.64	9.88
0.131 (maximum measured)	-32.19	9.88
Sensitivity	**539.5 dB/mm**	**Not applicable**
Dimensionless Sensitivity (%)	$\mathbf{539.5 \times \frac{0.128}{34.34} \times 100 = 201\%}$	**Not applicable**

2.5.2 Sensitivity Analysis for Surface Resistance

Results of sensitivity analysis for surface resistance are given in Figure 2.14 and Table 2.4. As seen, within the range of 66.8 Ω/sq and 83.3 Ω/sq values, increase in surface resistance increases amount of reflection loss and shifts the resonance frequency towards higher values. Sensitivity analysis for surface resistance showed that surface resistance has a significant effect on both resonance frequency and amount of reflection loss.

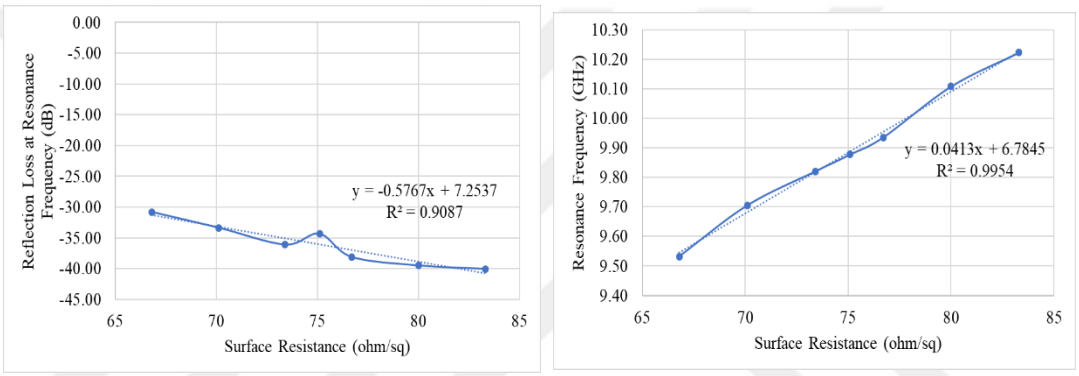

(a) (b)

Figure 2.14 Graphs of sensitivity analysis to determine effect of surface resistance on (a) reflection loss at resonance frequency, (b) resonance frequency

Table 2.4 Results of sensitivity analysis for surface resistance

Surface Resistance (Ω/sq)	**Reflection Loss at Resonance Frequency (dB)**	**Resonance Frequency (GHz)**
66.8 (minimum measured)	-30.81	9.53
70.1	-33.34	9.71
73.4	-36.09	9.82
75.1 (nominal)	-34.34	9.88
76.7	-38.10	9.94
80	-39.49	10.11
83.3 (maximum measured)	-40.05	10.22
Sensitivity	**0.5767 dB/(ohm/sq)**	**0.0413 GHz/(ohm/sq)**
Dimensionless Sensitivity (%)	$\mathbf{0.5767 \times \frac{75.1}{34.34} \times 100 = 126\%}$	$\mathbf{0.0413 \times \frac{75.1}{9.88} \times 100 = 31.4\%}$

2.5.3 Sensitivity Analysis for Ply Thickness

Results of sensitivity analysis for ply thickness can be found in Figure 2.15 and Table 2.5. As it can be realized, within the range of measured values for ply thickness (0.255 - 0.267 mm), reflection loss behavior considerably changes. Increase in ply thickness shifts resonance frequency to higher values and reduces amount of reflection loss drastically.

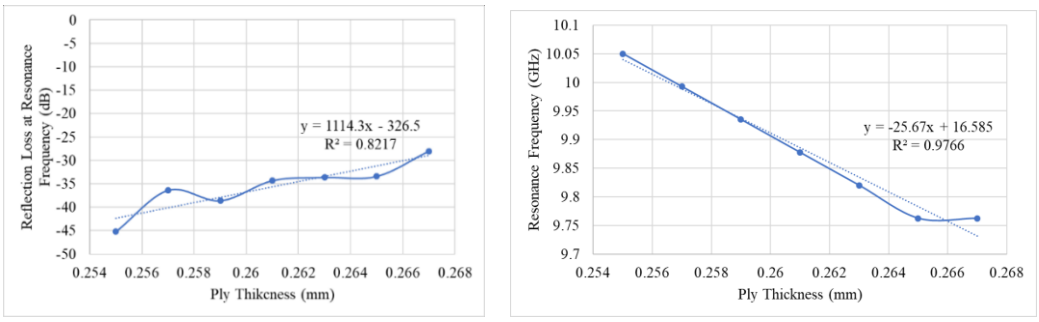

(a) (b)

Figure 2.15 Graphs of sensitivity analysis to determine effect of ply thickness on (a) reflection loss at resonance frequency, (b) resonance frequency

Table 2.5. Results of sensitivity analysis for ply thickness

Ply Thickness (mm)	**Reflection Loss at Resonance Frequency (dB)**	**Resonance Frequency (GHz)**
0.255 (minimum measured)	-45.21	10.05
0.257	-36.40	9.99
0.259	-38.62	9.94
0.261 (nominal)	-34.34	9.88
0.263	-33.67	9.82
0.265	-33.44	9.76
0.267 (maximum measured)	-28.04	9.76
Sensitivity	**1114.3 dB/mm**	**25.67 GHz/mm**
Dimensionless Sensitivity (%)	$\mathbf{1114.3 \times \frac{0.261}{34.34} \times 100 = 846.9\%}$	$\mathbf{25.67 \times \frac{0.261}{9.88} \times 100 = 67.8\%}$

2.5.1 Sensitivity Analysis for Dielectric Permittivity and Loss Tangent of GFREMP

Sensitivity analysis for dielectric permittivity of GFREMP was applied for dielectric permittivity constant and loss tangent values individually. As seen in Figure 2.16 and Table 2.6, increasing dielectric permittivity constant decreases reflection loss and also shifs reosnance frequency towards lower values. Although the dimensionless sensitivy is high, within the range of minimum and maximum measured dielectric permittivty constant values change in permittivity constant has a minor effect on reflection behavior of composite material. Similarly, when Figure 2.17 and Table 2.7 are evaluated it can be concluded that change in loss tangent between mininumum and maximum measured values do not have considerable effect.

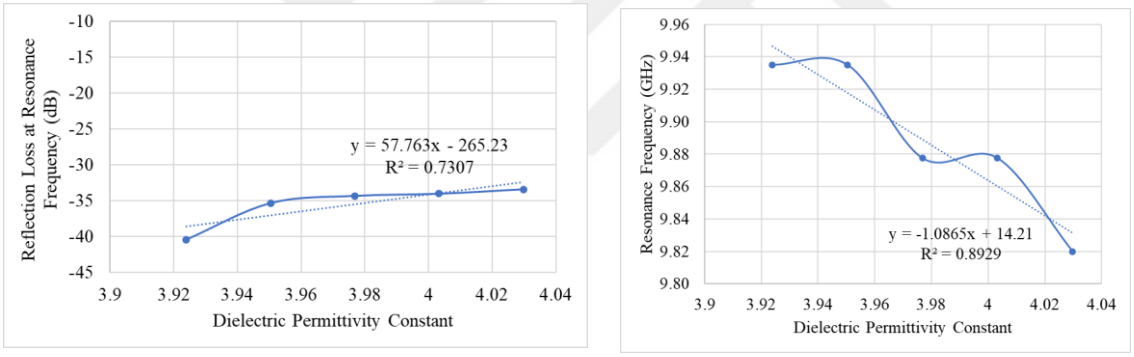

(a) (b)

Figure 2.16 Graphs of sensitivity analysis to determine effect of dielectric permittivity constant on (a) reflection loss at resonance frequency, (b) resonance frequency

Table 2.6 Results of sensitivity analysis for dielectric permittivity constant

Dielectric Permittivity Constant	**Reflection Loss at Resonance Frequency (dB)**	**Resonance Frequency (GHz)**
3.9239 (tanδ: 0.0049) (minimum measured)	-40.42	9.94
3.95035 (tanδ: 0.0049)	-35.35	9.94
3.9768 (tanδ: 0.0049) (nominal)	-34.34	9.88
4.003275 (tanδ: 0.0049)	-34.05	9.88
4.02975 (tanδ: 0.0049) (maximum measured)	-33.43	9.82
Sensitivity	**57.8 dB**	**1.09 GHz**
Dimensionless Sensitivity (%)	$\mathbf{57.8 \times \frac{3.9768}{34.34} \times 100 = 669.4\%}$	$\mathbf{1.09 \times \frac{3.9768}{9.88} \times 100 = 43.9\%}$

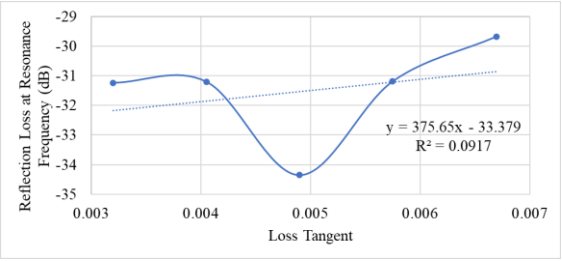

(a)

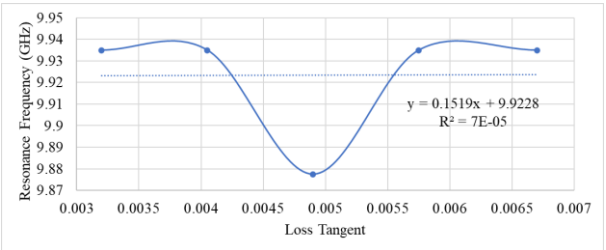

(b)

Figure 2.17 Graphs of sensitivity analysis to determine effect of loss tangent on (a) reflection loss at resonance frequency, (b) resonance frequency

Table 2.7 Results of sensitivity analysis for loss tangent

Loss Tangent	**Reflection Loss at Resonance Frequency (dB)**	**Resonance Frequency (GHz)**
tanδ: 0.0032, ($\varepsilon_r = 3.9768$) (minimum measured)	-31.24	9.94
tanδ: 0.00405, ($\varepsilon_r = 3.9768$)	-31.20	9.94
tanδ: 0.0049, ($\varepsilon_r = 3.9768$) (nominal)	-34.34	9.88
tanδ: 0.00575, ($\varepsilon_r = 3.9768$)	-31.19	9.94
tanδ: 0.0067, ($\varepsilon_r = 3.9768$) (maximum measured)	-29.68	9.94
Sensitivity	**375.7 dB**	**Not applicable**
Dimensionless Sensitivity (%)	$\mathbf{375.7 \times \frac{0.0049}{34.34} \times 100 = 5.36\%}$	**Not applicable**

Sensitivity analysis concluded that among all of the design parameters, surface resistance and ply thickness (and so spacer thickness) have major effect on reflection behavior of composite material. Therefore, to measure them accurately and to have a greate control over them during manufacturing play a substantial role in designing and achieving targeted absorbing property.

CHAPTER 3

EXPERIMENTAL PROCEDURE

3.1 Materials

A glass fiber reinforced epoxy matrix prepreg (GFREMP) system (VTP DA 100 EGU 280 T RC40) from SPM Prepreg Systems, Turkey was used to construct both substrate and top layer since it is a frequently used prepreg material in composite part production.

In order to have a perfect electric conducting layer, a carbon fiber reinforced epoxy matrix prepreg (CFREMP) system (VTP DA 100 CFA 200 3KP RC40) having the same epoxy matrix material with GFREMP system was used.

To form FSS layer, a conductive graphene ink from Haydale Graphene Industries was used since it is suitable for screen-printing process.

FSS pattern was applied to PES film.

3.2 Characterization to Design Composite Material with FSS Layer

As mentioned above, designing composite material with FSS layer was conducted after determining the dielectric permittivity of substrate, top layer and PES film materials, surface resistance of conductive ink and thickness of PES film.

3.2.1 Determination of Dielectric Permittivity of Substrate, Top Layer and PES Film Materials

Electromagnetic characterization of used materials (substrate, top layer and PES film material) was done by means of rectangular waveguide (Agilent WR90) and vector network analyzer (Agilent E8364) system shown in Figure 3.1. Test specimen was placed in the spacemen holder of waveguide which basically guides the electromagnetic waves thorough the specimen. Network analyzer calculates the dielectric permittivity and magnetic permeability by simply analyzing the applied and collected waves. It should be noted that magnetic permeability of the materials was assumed as 1, since they don't contain any magnetic particle.

Test specimens of GFREMP, which was used to form substrate and top layer, were produced by prepreg lay-up technique. To do so, 15 layers of GFREMP were laid-up and cured in woven. Curing cycle was 30 minutes at 90ºC and 2 hours at 120ºC with 3ºC/min heating and cooling rate. It is important specify that the same curing cycle was applied to all composite specimen and plate production due to the fact that curing cycle affects the crosslinking of epoxy matrix, which plays an important role on dielectric permittivity of composite material. Specimens were cut to 22.86 mm x 10.16 mm (Figure 3.1). 2 specimens were tested.

To measure dielectric permittivity of PES film, specimen was placed between two waveguide such that air fills the gap in the specimen holder.

(a) 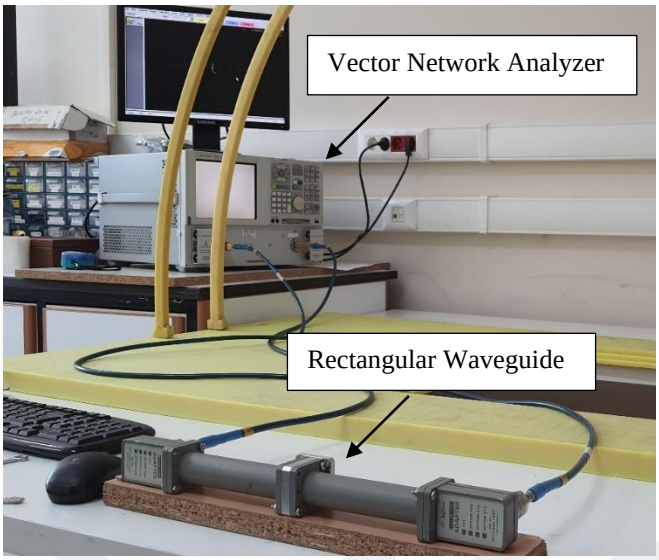

(b) 

Figure 3.1 (a) Test setup for determination of dielectric permittivity of substrate and top layer material (b) test specimen of GFREMP

3.2.2 Determination of Surface Resistance of Conductive Ink

Surface resistance was measured with 4-point-probe technique (Lucas Labs Pro4). As the name implies, there are 4 probes which have equal distance between them. Current is applied through the 2 outer probes while 2 inner probes measure the voltage drop. Surface resistance is calculated using Equation 3.1 [37].

$$R_s = \frac{\pi}{ln2}\frac{\Delta V}{I} \tag{3.1.1}$$

Specimens were produced with screen printing method on PES film with a size of 5 mm x 25 mm. In order to see the scattering of the results, production and tests were conducted for several times. Details of screen printing method is explained below:

1. Screen preparation:
    a. A film mask, having the desired pattern of FSS, was produced by means of printing technique.

b. Screen was formed by stretching and fixing a silk fabric on a metal frame.
c. A UV-curable emulsion mixture was poured on this mold. The film mask was placed on that screen before exposing UV-light. Since UV-light could not pass through the film mask, emulsion just under the pattern area could not be consolidated while the rest was cured.
d. Screen was washed by water so that uncured emulsion chemical was removed. The cured emulsion mixture filled the pores on the silk screen, which doesn't allow the conductive ink to pass below the screen in order to form the gap between the unit cell pattern. On the other hand, since the film mask blocked the certain areas such that the pores forming the unit cell pattern were left empty allowing the conducting ink to be passed through the screen.
e. The obtained screen having the FSS pattern can be seen in Figure 3.2.a.

2. FSS layer production with screen printing:
    a. A semi automatic screen printing machine was used (Figure 3.2) in this work.
    b. Conductive ink was placed on the screen. A squeegee was moved from one side to the other on the screen so that conductive ink was passed through the silk and formed unit cell pattern on PES film.
    c. FSS layer was then cured in oven for 30 minutes at 100ºC.

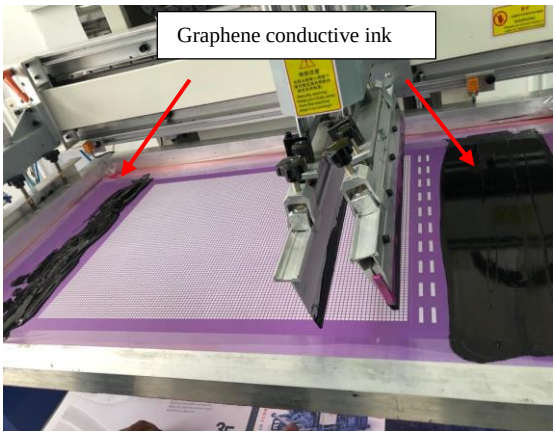

(a)

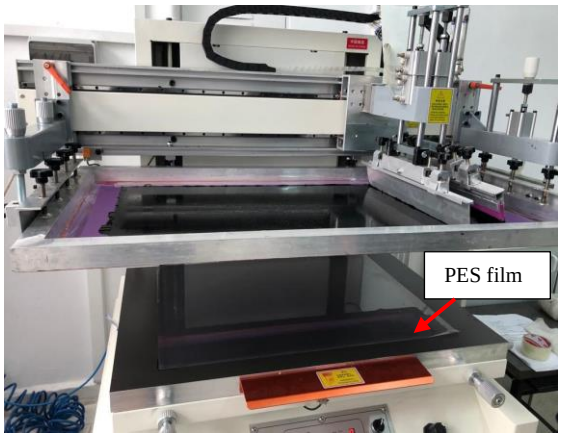

(b)

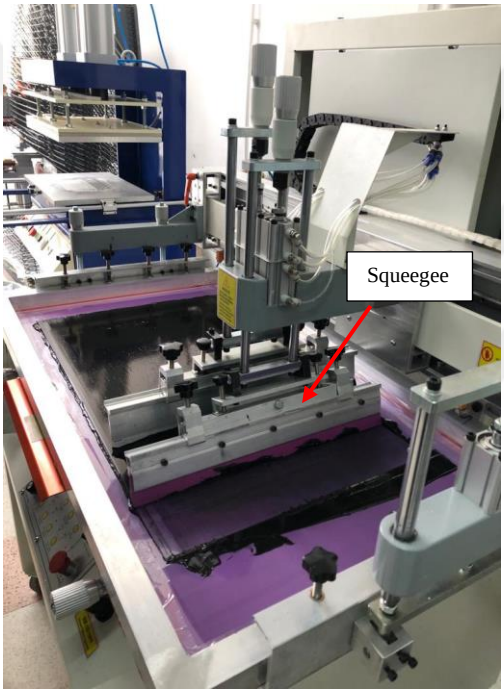

(c)

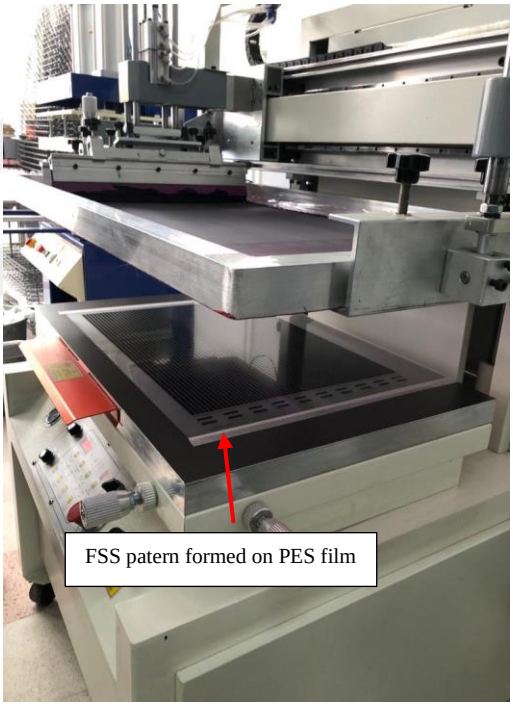

(d)

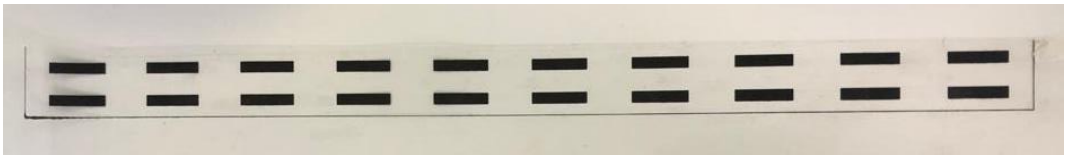

(e)

Figure 3.2 Production steps of screen printing. (a) screen having the desired FSS pattern, (b) semi automatic screen printing machine (just before screen printing), (c) squeegee moving from one side to the other (during the screen printing) (d) obtained FSS on PES film (after screen printing), (e) sample for surface resistance measurement

3.2.3 Determination of PES Film Thickness

Thickness of PES film was measured with digital micrometer (Mitutoyo, IP65).

Figure 3.3 PES film thickness measurement with micrometer

3.2.4 Determination of Cured Ply Thickness

Since the composite material is manufactured by means of prepreg lay-up process, the thickness of single prepreg layer, that is called as ply thickness, controls the total thickness of spacer and top layer material. To determine the cured ply thickness, 12 layers of GFREMP were laid-up and cured in woven with curing cycle of 30 minutes at 90ºC and 2 hours at 120ºC with 3ºC/min heating and cooling rate. Thickness of that composite plate was measured with digital micrometer (Mitutoyo, IP65) and divided in 12 to obtain ply thickness.

3.3 Characterization for Mechanical, Thermal and Physical Properties of Composite Material

In order to determine the effect of FSS layer on mechanical (tensile, flexural and shear properties), thermal (glass transition temperature) and physical (fiber content and density) properties of composite material, reference plates (composite without FSS layer) and composite plates with FSS layer were produced and tested. Composite plates were manufactured by prepreg lay-up and vacuum bagging technique and details were already given previously. Differently from composite plate manufacturing for radar absorbing property characterization, FSS layer was

inserted in the middle plane of composite plates. Moreover, thickness of test specimens was arranged in accordance with ASTM test standards.

3.3.1 Determination of Tensile Properties

Tensile strength and elastic modulus of composite plates (with and without FSS layer) were examined by applying tensile test according to ASTM D3039 test standard. Prepreg lay-up configuration of composite plates are as follow:

- Reference composite plate: 10 layers of GFREMP (unidirectional)
- Composite plate with FSS layer: 5 layers of GFREMP + FSS layer + 5 layers of GFREMP (unidirectional)

(a) 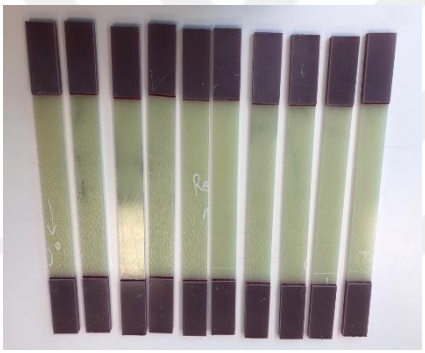 (b) 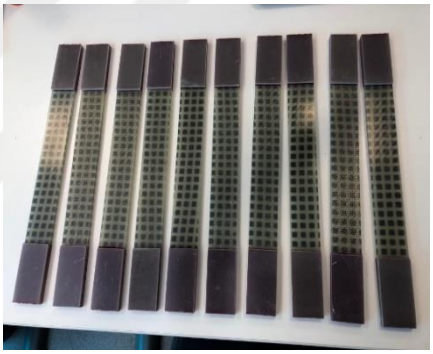

Figure 3.4 Tensile test coupons. (a) Reference material test coupons, (b) Composite with FSS layer test coupons

Obtained composite plates with and without FSS layer had 2.6 mm and 2.73 mm thickness respectively. Test coupons were cut using composite cutting bench (Extec Labcut 5000) to have 250 x 25 mm in size. Tab material was used to prevent damage due to the pressure applied by grips. 10 specimens of each composite material (Figure 3.4) were produced and tested.

Gage length was selected as 50 mm. Video extensometer was used for strain measurement. Since video extensometer follows the gage markers' movement, test coupons were painted with black pen to increase the contrast (Figure 3.5). 2 mm/min

rate was applied during the test as specified in ASTM D3039. Instron 5982 tensile test device was used in this work.

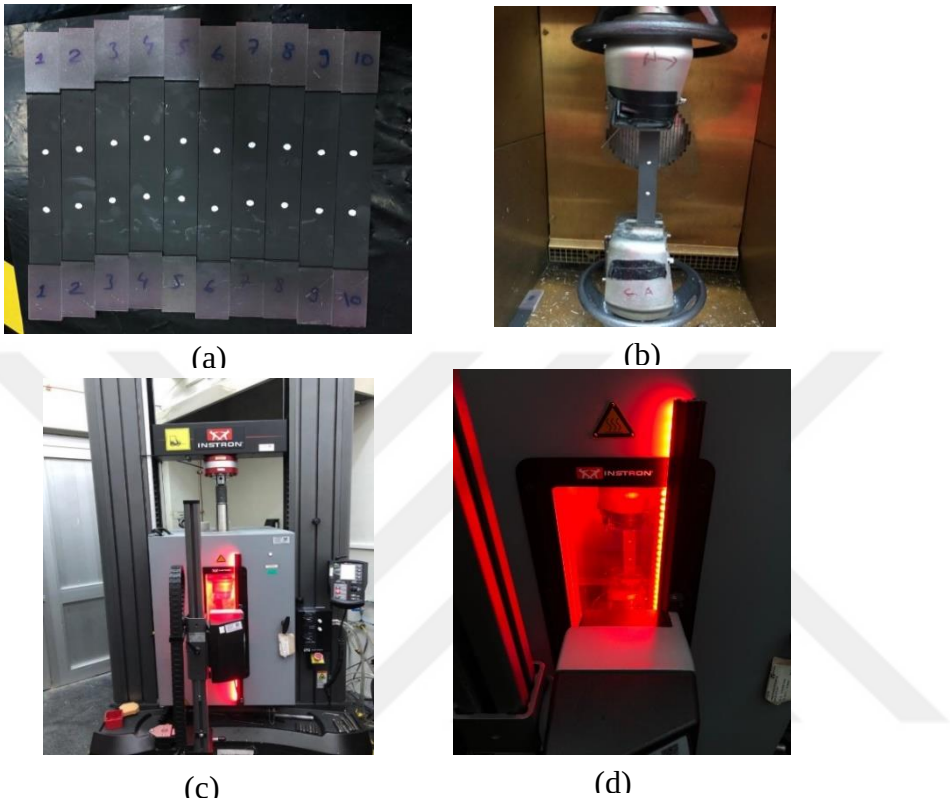

Figure 3.5 Tensile test of the specimens. (a) Painted and gage length marked coupons, (b) tensile grips, (c) Instron tensile test device, (c) strain measurement with video extensometer

3.3.2 Determination of Flexural Properties

3-point-bending test, in accordance with ASTM D790, was conducted to both the reference material (without FSS) and composite material with FSS layer. Prepreg lay-up configuration of composite plates were the same as in tensile testing, which was:

- Reference composite plate: 10 layers of GFREMP
- Composite plate with FSS layer: 5 layers of GFREMP + FSS layer + 5 layers of GFREMP.

Test plates were cut in 90 mm x 12 mm size for coupon preparation. 16:1 span length to thickness ratio was applied as indicated in ASTM D790 standard. Since thickness of reference material and composite material with FSS layer was 2.60 mm and 2.73 mm respectively, span length was calculated as 41.6 mm and 43.68 mm. As specified in ASTM D790, Equation 3.4.1 was used to evaluate the testing rate, where R is the applied rate, Z equals to 0.01, L is the support span length and d is the thickness of test coupons. Rates were calculated as 1.109 mm/min and 1.165 mm/min for reference material and composite material with FSS layer respectively.

$$R = \frac{ZL^2}{6d} \tag{3.4.1}$$

(a)  (b) 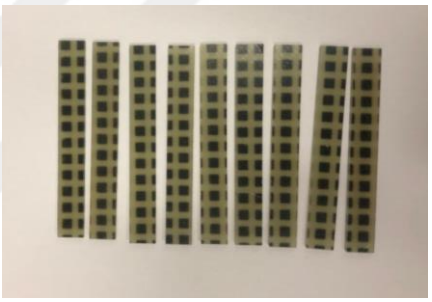

Figure 3.6 3-point-bending test coupons. (a) Reference material test coupons, (b) Composite with FSS layer test coupons

9 test coupons (Figure 3.6) of each composite material were tested using Instron 5500R test device (Figure 3.7).

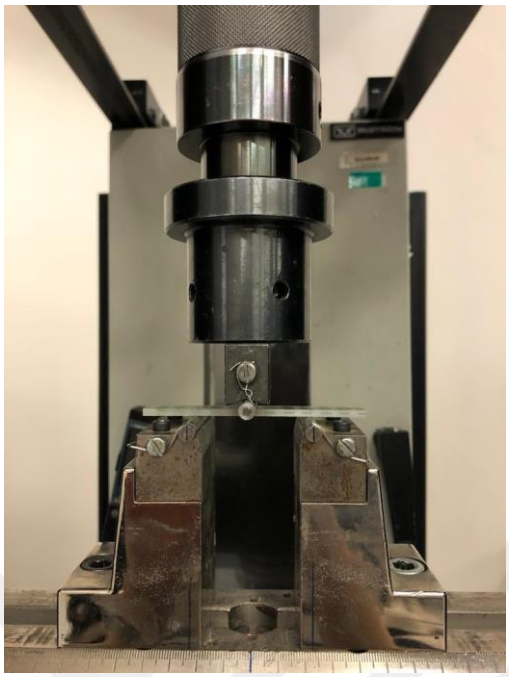

Figure 3.7 Test device for flexural property determination

3.3.3 Determination of Shear Properties

ASTM 3518 test standard was followed to test shear properties of composite material. Prepreg lay-up configuration was different from the tensile test plates:

- Reference composite plate: 8 layers of GFREMP ($[\pm 45]_{4s}$)
- Composite plate with FSS layer: 4 layers of GFREMP + FSS layer + 4 layers of GFREMP ($[\pm 45]_{4s}$)

Thicknesses of test plates were 2.08 mm and 2.21 mm for reference material and composite material with FSS layer. Test plates were cut to obtain 250 mm x 25 mm test coupons. Tab material was pasted to prevent grip damage. Longitudinal and latera strain were measured using video extensometer. 2 mm/min testing rate was applied and Instron 5982 were used in this test. 10 test coupons of each composite material were tested (Figure 3.8).

Figure 3.8 Shear test coupons which were marked to measure both longitudinal and lateral strain

3.3.4 Determination of Glass Transition Temperature

ASTM D7028 test standard was applied to determine glass transition temperature of composite material. Test coupons were cut from the composite plates which were produced for tensile testing. Test coupons were in size of 55 mm x 12.5 mm. TA Instruments ARESG2 device was used to test 2 coupons of each composite material.

3.3.5 Determination of Density and Fiber Content

Test specimens were cut from the plates (2.60 mm and 2.73 mm thick plates) which were manufactured for tensile testing. Firstly, density of test specimens, 55 mm x 12.5 mm in size, was measured in accordance with ASTM D792 (using Mettler Toledo XPR205) and then, the same specimens were used for fiber content measurement (ASTM D3171). 6 test specimens of each composite material were tested to determine density and fiber content.

3.4 Characterization for Radar Absorbing Property

After determining the design parameters for radar absorbing composite material with finite element analysis, composite plate with FSS layer was manufactured for experimental verification. FSS layer was produced with screen printing method of which details were given above. After that, composite plate having FSS layer was produced by prepreg lay-up technique. 2 layers of CFREMP were used for perfect electric conducting layer. On top of CFREMPs, 10 layers of GFREMP were laid up to form 2.61 mm thick substrate. FSS layer was placed on the GFREMPs. Finally, 1 layer of GFREMP was laid up as the top layer. This system was cured in oven with curing cycle of 30 minutes at 90ºC and 2 hours at 120ºC with 3ºC/hr heating and cooling rate. The obtained plate was 450 x 650 x 2.61 mm in size. Manufacturing steps and produced composite plate can be seen in Figure 3.9 and Figure 3.10.

NRL Arch Method was followed to measure frequency vs reflection loss behavior. Two horn antennas (ATM WR90) were placed on an arch having 100 cm outer radius. In order to satisfy 0º incidence angle, the distance between the antennas (10 cm) was arranged as small as possible in such a way that they didn't interfere with each other. In order to analyze the applied and reflected electromagnetic waves, vector network analyzer (Agilent E8364) was used. Measurements were conducted in X band frequency range (8.2 – 12.4 GHz). Pyramidal absorbers were placed around the test specimen with the aim of preventing reflections from the ground surface. Prior to measuring the composite plate sample, copper pate, which reflects electromagnetic waves perfectly, was tested. The reflection of copper plate was taken as reference. Reflection loss of composite plate was calculated, by using vector network analyzer, relative to the copper plate. Test setup is shown in Figure 3.11.

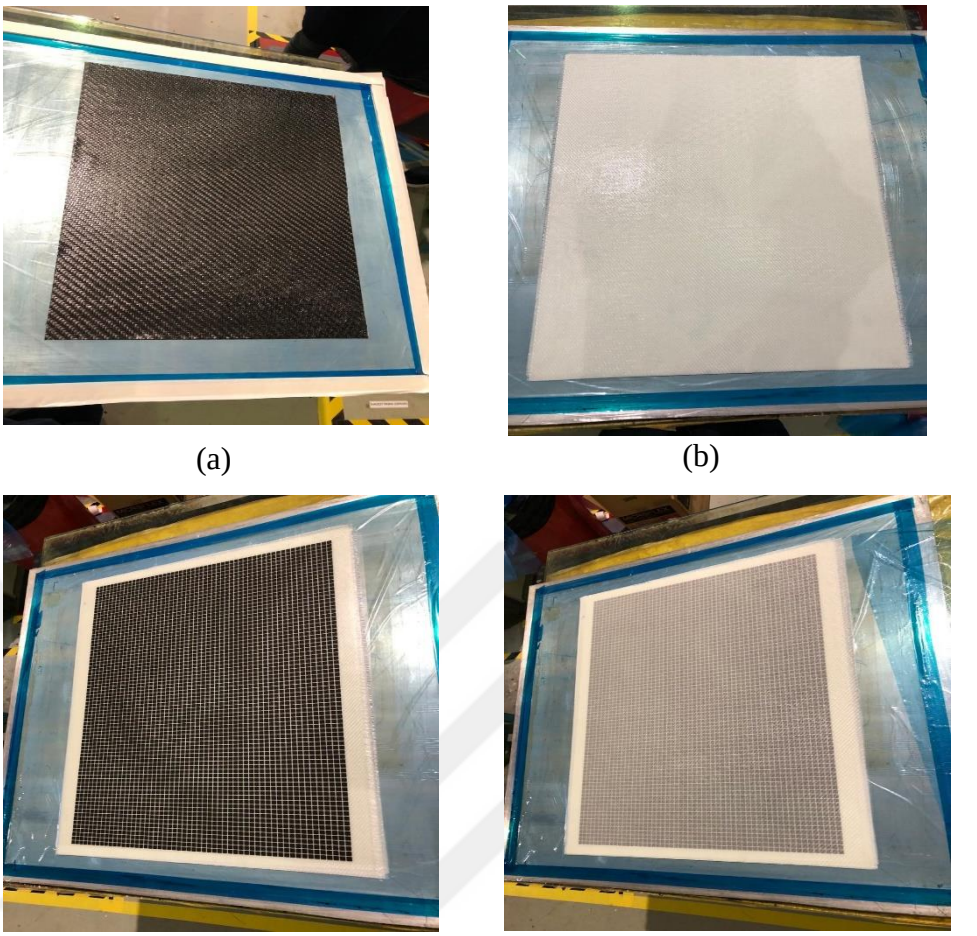

Figure 3.9 Composite plate production steps. (a) CFREMP lay-up as perfect electric conducting layer, (b) GFREMP lay-up to form substrate, (c) placing FSS layer, (d) GFREMP lay-up as top layer, (e) vacuum bagging, (d) oven curing

Figure 3.10 Produced composite plate 450 x 650 x 2.61 mm in size

Figure 3.11 Test setup for radar absorbing property measurement

CHAPTER 4

RESULTS AND DISCUSSION

4.1 Test Results of Characterization to Design Composite with FSS Layer

4.1.1 Determination of Dielectric Permittivity of Substrate, Top Layer and PES film Materials

Dielectric permittivity measurement results of composite material and PES film are presented in Figure 4.1 and Figure 4.2, respectively. For composite material, average of the results ($\varepsilon_r = 3.9768 - j0.01949$) was used in finite element analysis. For PES film material, it was realized that result ($\varepsilon_r = 3.2 - j0.096$) was the same as the property of "*polyester*" in material library in Ansys HFSS tool.

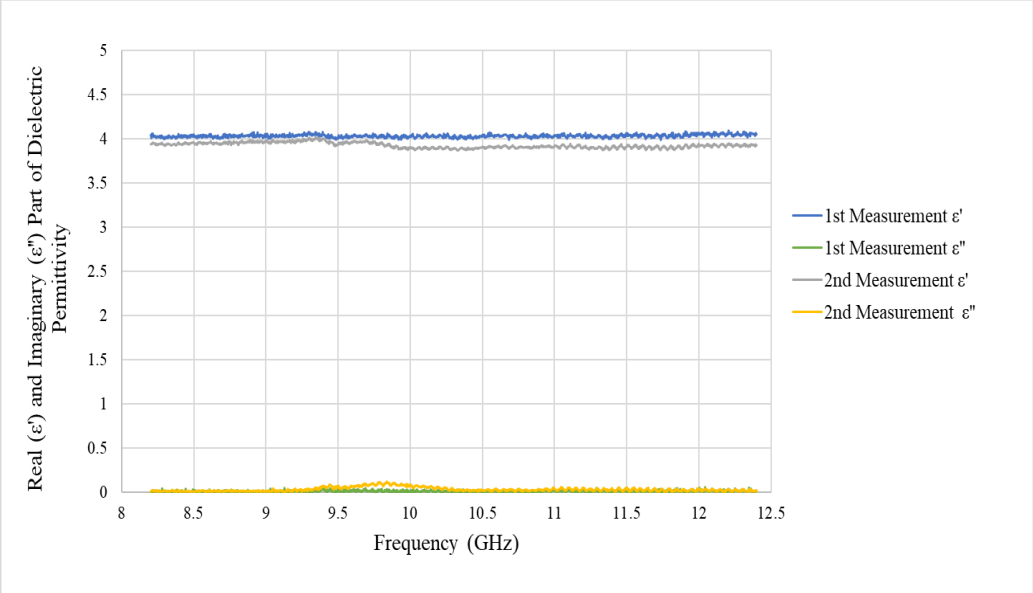

Figure 4.1 Result of dielectric permittivity measurement of substrate and top layer material

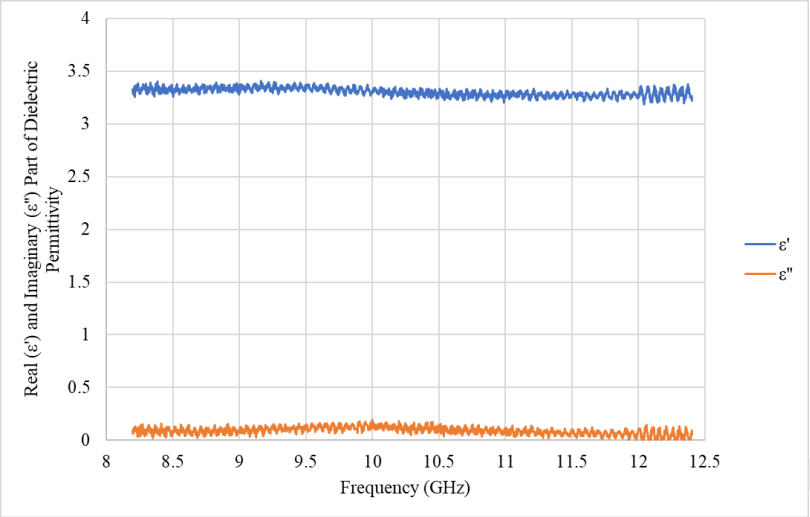

Figure 4.2 Result of dielectric permittivity measurement of PES film

4.1.2 Determination of Surface Resistance of Conductive Ink

Surface resistance measurement by 4-point-probe technique was performed for several samples which belonged to 2 different production batches. Results can be seen in Table 4.1. Average surface resistance values for 2 production batch are 75.8 Ω/sq and 74.3 Ω/sq, which are consistent with each other. In FEA analysis, average of all the measurement results, which was 75.1 Ω/sq, were used as surface resistance parameter. However, it can be seen that variation coefficient of each production batches are 6.6%. This result may be a consequence of inhomogeneous pressing in the screen printing process and/or inhomogeneous temperature distribution in oven during curing of conductive ink.

Table 4.1 Surface resistance measurement results

Sample Number	1st Production Batch		2nd Production Batch	
	ΔV/I (Ω)	R_s (Ω/sq)	ΔV/I (Ω)	R_s (Ω/sq)
1	15.6	70.8	16.1	72.7
2	17.4	78.7	18.3	82.8
3	17.8	80.8	17.3	78.5
4	16.2	73.3	15.2	68.7
5	17.5	79.1	14.7	66.8
6	16.7	75.6	16.5	74.8
7	15.5	70.4	17.3	78.5
8	18.4	83.3	16.6	75.3
9	16.2	73.3	15.5	70.4
10	15.1	68.4	16.4	74.3
11	17.9	80.7	-	-
Average	**16.6**	**75.8**	**16.4**	**74.3**
Standard Deviation	**1.1**	**0.7**	**1.1**	**4.9**
Variation Coefficient	**6.6%**	**6.6%**	**6.6%**	**6.6%**

4.1.3 Determination of PES Film Thickness

Results of thickness measurement of 2 different PES film samples using micrometer are given in Table 4.2. Average values of samples were 0.129 mm and 0.127 mm, which had low variation coefficient (2% and 1.8%) and were very close to each other. In finite element analysis, the average value of all of the measurements were considered and 0.128 mm was taken as PES film thickness.

Table 4.2 PES film thickness measurement results

Measurement	1st Sample (mm)	2nd Sample (mm)
1	0.129	0.129
2	0.127	0.129
3	0.131	0.124
4	0.125	0.129
5	0.131	0.126
Average	**0.129**	**0.127**
Standard Deviation	**0.003**	**0.002**
Variation Coefficient	**2.0%**	**1.8%**

4.1.4 Determination of Cured Ply Thickness

Composite plate thickness was measured from different positions to see the variation in cured ply thickness. Results are listed in Table 4.3. Cured ply thickness was determined as 0.261 mm.

Table 4.3 Cured ply thickness measurement results

Measurement	Composite Plate Thickness (mm)	Cured Ply Thickness (mm)
1	3.17	0.264
2	3.2	0.267
3	3.2	0.267
4	3.11	0.259
5	3.06	0.255
6	3.16	0.263
7	3.12	0.260
8	3.11	0.259
9	3.19	0.266
10	3.12	0.260
11	3.08	0.257
12	3.13	0.261
13	3.07	0.256
14	3.15	0.263
1	3.15	0.263
16	3.13	0.261
17	3.14	0.262
18	3.17	0.264
Average	**3.14**	**0.261**
Standard Deviation	**0.04**	**0.003**
Variation Coefficient	**1.3%**	**1.3%**

4.2 Test Result of Characterization for Mechanical, Thermal and Physical Properties of Composite Material

4.2.1 Determination of Tensile Properties

Stress vs strain graphs of reference material (composite without FSS layer) and composite with FSS layer material are given in Figure 4.3 and Figure 4.4. Also, test results are summarized in Table 4.4 and Table 4.5. It should be noted that chord modulus, which is the modulus calculated within the 0.001-0.003 mm/mm strain interval, was evaluated since ASTM D3039 test standard indicates that chord modulus should be considered as tensile property for material design.

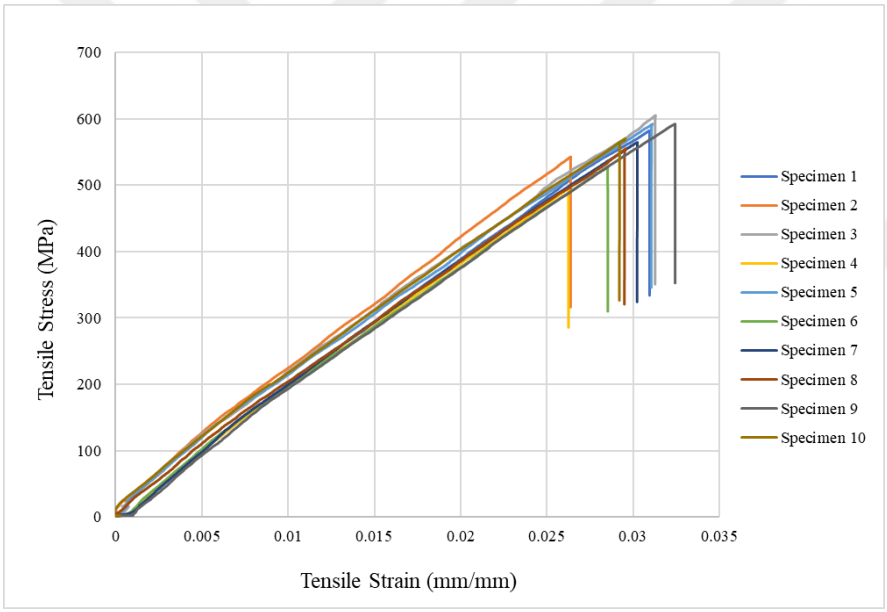

Figure 4.3 Tensile Stress – Strain graphs of reference composite material

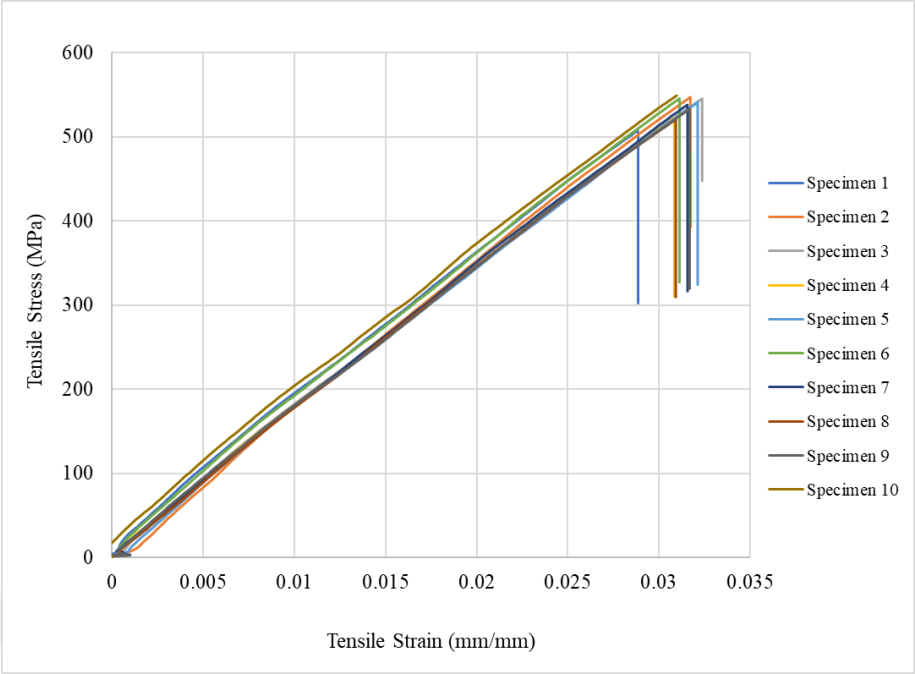

Figure 4.4 Tensile Stress – Strain graphs of composite material with FSS layer

Table 4.4 Reference composite material tensile test results

Specimen	Maximum Load (kN)	Tensile Strength (MPa)	Chord Modulus (GPa)
1	37	582	23
2	32	543	23
3	37	604	23
4	31	495	24
5	37	591	23
6	33	528	24
7	35	564	23
8	35	553	20
9	37	592	23
10	36	570	22
Average	**35**	**562**	**23**
Standard Deviation	**2**	**33**	**1**
Variation Coefficient	**6%**	**6%**	**6%**

Table 4.5 Composite material with FSS layer tensile test results

Specimen	Maximum Load (kN)	Tensile Strength (MPa)	Chord Modulus (GPa)
1	35	508	19
2	37	547	19
3	37	545	20
4	36	522	17
5	37	541	20
6	37	546	19
7	37	538	26
8	36	521	17
9	37	533	19
10	38	551	19
Average	**37**	**535**	**20**
Standard Deviation	**1**	**14**	**3**
Variation Coefficient	**2%**	**3%**	**13%**

Tensile strength of reference material and composite with FSS layer were determined as 562 MPa and 535 MPa respectively. There is 4.8% decrease in tensile strength of composite material due to the PES film. Similarly, chord modulus of composite material diminished from 23 GPa to 20 GPa. The reason behind it can be easily seen when failure behaviors of specimens are examined (Figure 4.5). During tensile testing, reference material failed by means of fiber breakage. However, composite with FSS material exhibited delamination on PES film layer in addition to the fiber breakage. This delamination led to earlier failure of composite with FSS material. Although tensile properties got worsen due to the PES film, the reductions in properties (27 MPa in tensile strength and 3 GPa in chord modulus) are relatively small and tensile properties of composite with FSS layer can be considered as acceptable.

(a)

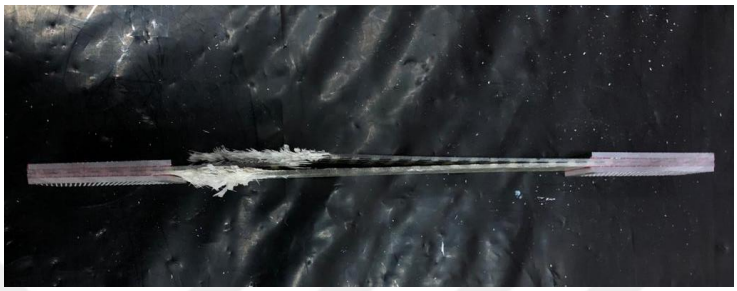

(b)

Figure 4.5 Failure behavior of tensile specimens. (a) reference material, (b) composite material with FSS layer

4.2.2 Determination of Flexural Properties

Flexural stress and strain of the composite materials was calculated using Equation 4.2.1 and Equation 4.2.2, as specified in ASTM D790 test standard. In these equations, P is the load at a given point, L is the support span length, D is deflection, b is width and d is thickness of the tested specimen. Chord modulus was calculated for all specimens within 0.01-0.03 strain range. Flexural stress vs strain graphs for reference and composite with FSS layer are given in Figure 4.6 and Figure 4.7.

$$\sigma_f = 3\,PL/2bd^2 \quad (4.2.1)$$

$$\varepsilon_f = 6\,Dd/L^2 \quad (4.2.2)$$

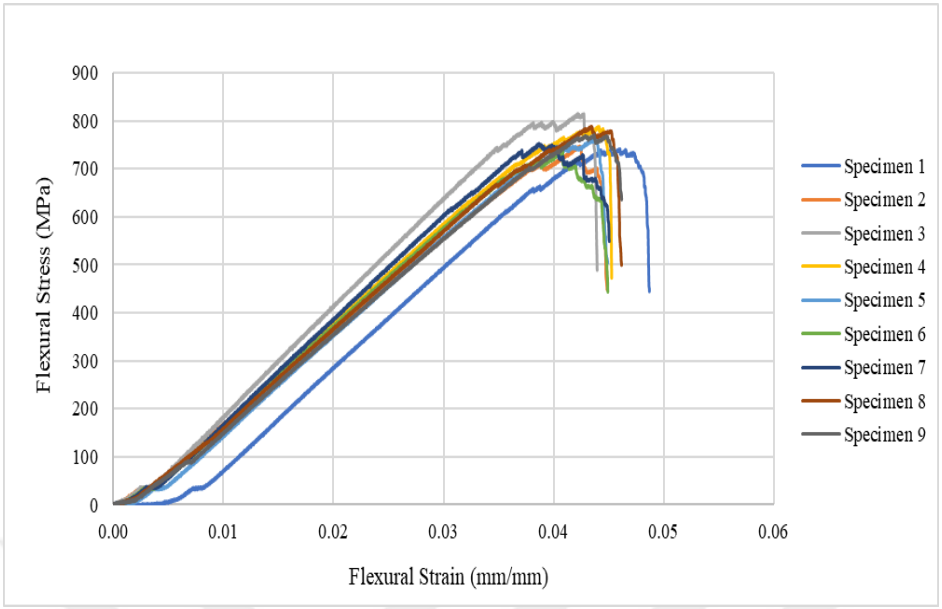

Figure 4.6 Flexural Stress – Strain graphs of reference composite material

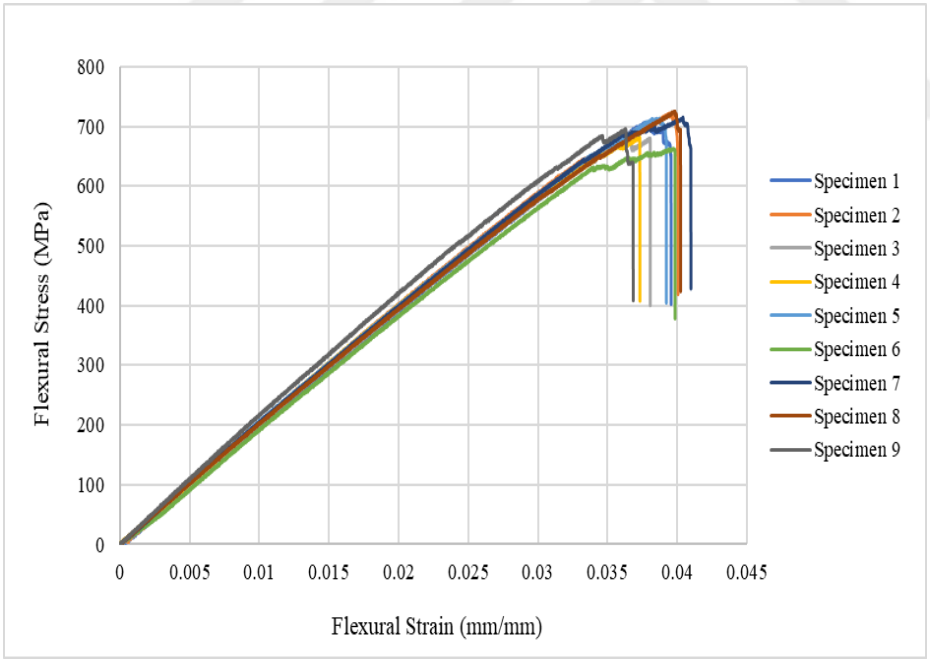

Figure 4.7 Flexural Stress – Strain graphs of composite material with FSS layer

3-point-bending test results for reference composite material and composite with FSS material are given in Table 4.6 and Table 4.7. Flexural strength and modulus of reference composite material was determined as 767 MPa and 21.0 GPa, while that of composite with FSS layer was found as 699 MPa and 19.0 GPa. There is 8.9% (68 MPa) decrease in flexural strength and 9.5% (2 GPa) reduction in flexural modulus due to existence of FSS layer, which results in delamination on PES film as it can be seen in Figure 4.8. However, flexural properties of composite with FSS layer can still be considered as sufficient for designing structural composite materials.

Table 4.6 Reference composite material 3-point-bending test results

Specimen	Maximum Load (kN)	Flexural Strength (MPa)	Chord Modulus (GPa)
1	0.894	741	21.2
2	0.940	747	19.5
3	0.936	815	22.8
4	0.984	788	20.9
5	0.939	760	20.7
6	0.875	739	20.7
7	0.880	752	21.8
8	0.949	788	20.6
9	0.944	771	20.3
Average	**0.93**	**767**	**21.0**
Standard Deviation	**0.04**	**26**	**0.9**
Variation Coefficient	**4%**	**3%**	**4%**

Table 4.7 Composite material with FSS layer 3-point-bending test results

Specimen	Maximum Load (kN)	Flexural Strength (MPa)	Chord Modulus (GPa)
1	0.971	707	19.0
2	0.979	722	19.3
3	0.936	681	18.7
4	0.933	694	18.9
5	0.981	713	19.0
6	0.918	663	18.7
7	0.984	716	19.1
8	0.995	725	18.7
9	0.923	666	19.6
Average	**0.96**	**699**	**19.0**
Standard Deviation	**0.03**	**24**	**0.3**
Variation Coefficient	**3%**	**3%**	**2%**

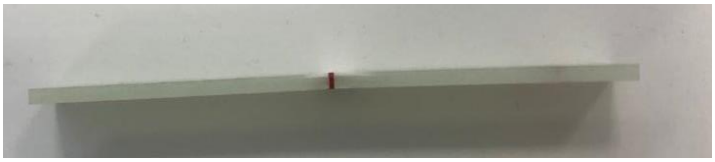

(a)

(b)

Figure 4.8 Failure behavior of 3-point-bending test specimens. (a) reference material, (b) composite material with FSS layer

4.2.3 Determination of Shear Properties

In ASTM D3518 test standard, it is indicated that 1.5º fiber scissoring should be the deformation limit for engineering design purposes and so, the test should be terminated at 5% shear strain level and maximum shear stress must be accepted as stress value corresponding to 5% shear strain, even though test specimen does not fail at this strain level. Therefore, to determine shear strength of composite material, this specified rule was followed in this work.

Shear stress and strain was calculated using Equation 4.2.3 and Equation 4.2.4 given in ASTM 3518 test standard. Here, P is the load, A is the cross-sectional area, ϵ_{xi} is longitudinal normal strain and ϵ_{yi} is lateral normal strain.

$$\tau_{12i} = \frac{P_i}{2A} \tag{4.2.3}$$

$$\gamma_{12i} = \epsilon_{xi} - \epsilon_{yi} \tag{4.2.4}$$

Shear stress vs strain graphs are given in Figure 4.9 and Figure 4.10. Also, test results are summarized in Table 4.8 and Table 4.9. It should be noted that, test results were terminated at 5% shear strain (50000 $\mu\epsilon$) and shear strength was calculated at that strain value. Furthermore, shear chord modulus of elasticity was calculated within 2000 to 6000 $\mu\epsilon$ strain range as stated in ASTM D3518 standard.

Shear strength and shear chord modulus of refence material was obtained as 56 MPa and 3.0 GPa. Composite material with FSS layer had 55 MPa shear strength and 2.9 GPa shear chord modulus. Although there occurred delamination during failure (Figure 4.11), test results show that placing PES film as FSS layer did not have negative effect on shear properties of composite material.

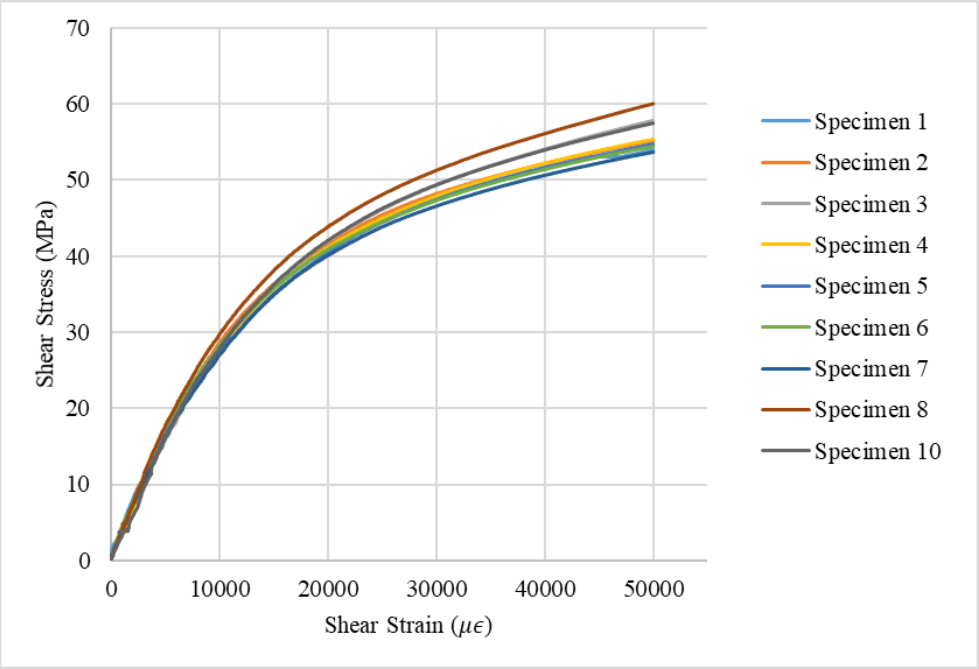

Figure 4.9 Shear Stress – Strain graphs of reference composite material

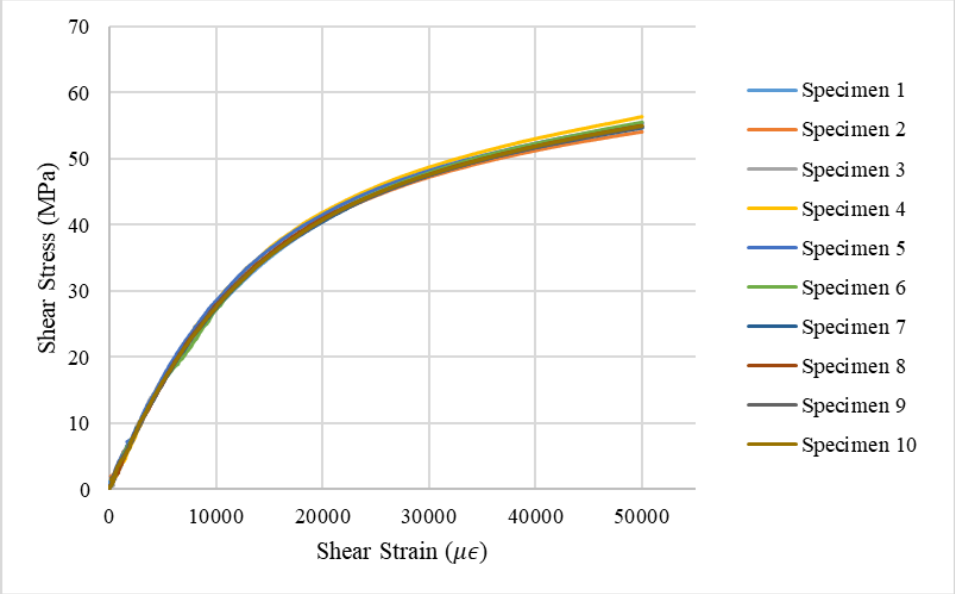

Figure 4.10 Shear Stress – Strain graphs of composite material with FSS layer

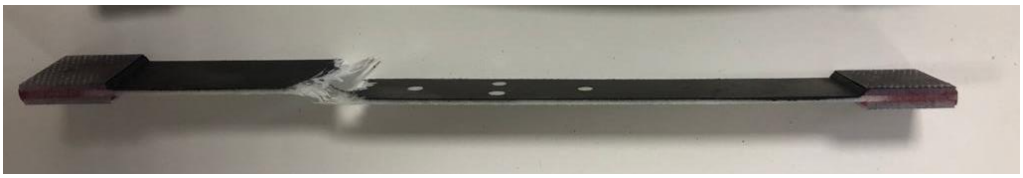

(a)

(b)

Figure 4.11 Failure behavior of shear test specimens. (a) reference material, (b) composite material with FSS layer

Table 4.8 Reference composite material shear test results

Specimen	Shear Strength (MPa)	Shear Chord Modulus of Elasticity (GPa)
1	54	2.8
2	55	3.0
3	58	2.7
4	55	3.1
5	55	2.8
6	54	3.1
7	54	2.9
8	60	3.3
9	54	2.9
10	57	3.3
Average	**56**	**3.0**
Standard Deviation	**2**	**0.2**
Variation Coefficient	**4%**	**7%**

Table 4.9 Composite material with FSS layer shear test results

Specimen	Shear Strength (MPa)	Shear Chord Modulus of Elasticity (GPa)
1	55	2.9
2	54	2.9
3	55	2.9
4	56	3.2
5	55	3.0
6	56	2.8
7	55	2.9
8	55	3.0
9	55	3.0
10	55	2.9
Average	**55**	**2.9**
Standard Deviation	**1**	**0.1**
Variation Coefficient	**1%**	**4%**

4.2.4 Determination of Glass Transition Temperature

Test result of dynamic mechanical analysis measurements of reference material and composite with FSS layer can be seen in Figure 4.12 and Figure 4.13. Through the glass transition stage, there occurs considerable decrease in storage modulus. As indicated in ASTM D7028 test standard, two tangent lines of storage modulus curve were drawn and glass transition temperatures were determined as the intersection of these lines. Glass transition temperatures of reference composite material and composite with FSS layer were found as 118.4 °C and 118.3 ºC respectively. It can be concluded that presence of PES film for FSS layer does not affect glass transition temperature of composite material.

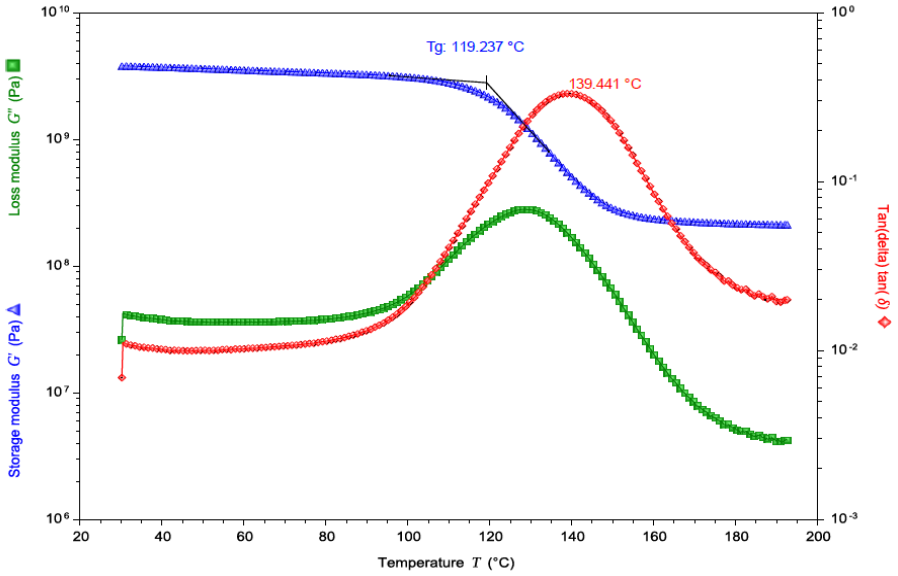

(a)

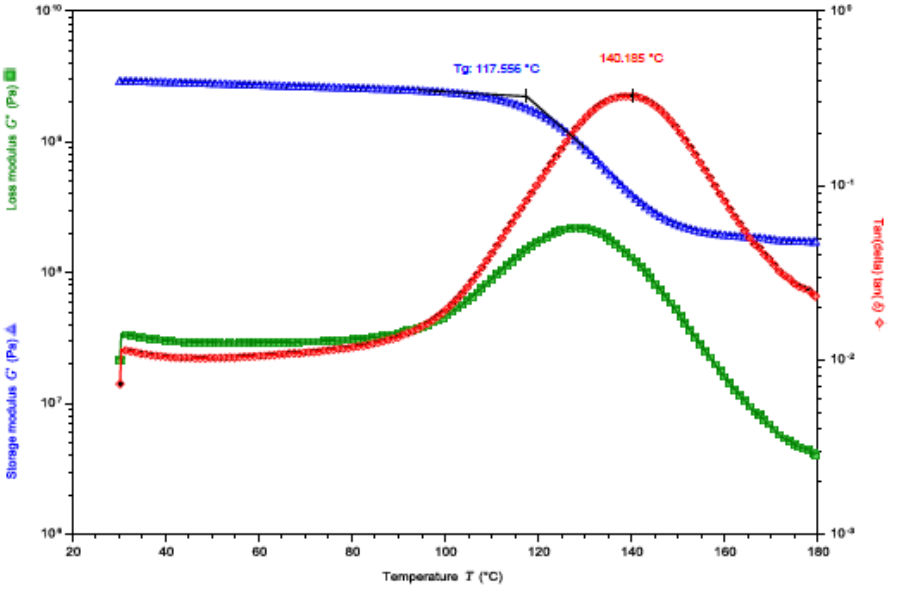

(b)

Figure 4.12 Dynamic mechanical analysis measurement test results of reference composite material (a)1st sample, (b) 2nd sample

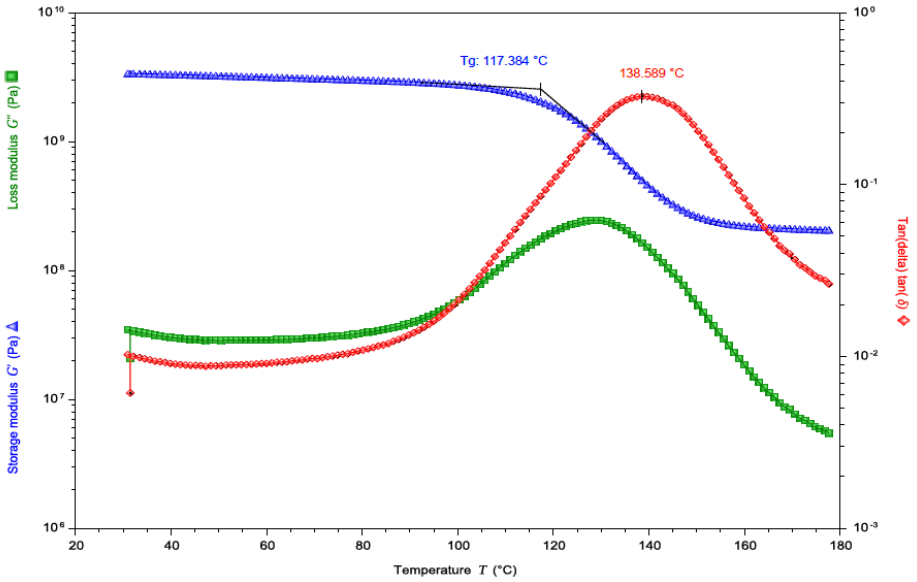

(a)

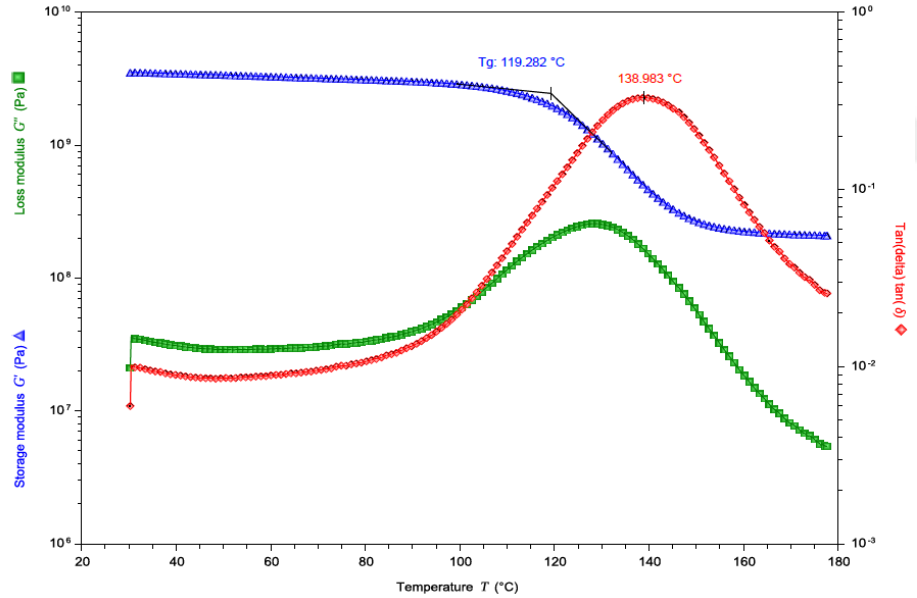

(b)

Figure 4.13 Dynamic mechanical analysis measurement test results of composite material with FSS layer (a) 1st sample, (b) 2nd sample

4.2.5 Determination of Density and Fiber Content

Test results of density and fiber content measurements are given in Table 4.10 and Table 4.11. Reference composite material's density and fiber content were determined as 1.807 g/cm^3 and 63.65 wt%. Composite with FSS layer material's density and fiber were found as 1.759 g/cm^3 and 59.43 wt%, which are smaller than that of reference composite material due to presence of PES film.

Table 4.10 Density and fiber content measurement results of reference composite material

Specimen	Density (g/cm^3)	Fiber Content (wt%)
1	1.808	63.62
2	1.797	63.82
3	1.795	63.39
4	1.812	63.83
5	1.809	63.68
6	1.820	63.54
Average	**1.807**	**63.65**
Standard Deviation	**0.009**	**0.17**
Variation Coefficient	**0.52%**	**0.3%**

Table 4.11 Density and fiber content measurement results of composite material with FSS layer

Specimen	Density (g/cm^3)	Fiber Content (wt%)
1	1.740	59.84
2	1.770	59.70
3	1.778	60.01
4	1.784	60.14
5	1.745	60.23
6	1.742	56.62
Average	**1.759**	**59.43**
Standard Deviation	**0.019**	**1.38**
Variation Coefficient	**1%**	**2%**

4.3 Test Result of Characterization of Radar Absorbing Property

Finite element analysis and characterization results of reflection loss are given in Figure 4.14. As seen, there is a significant deviation from the designed composite material.

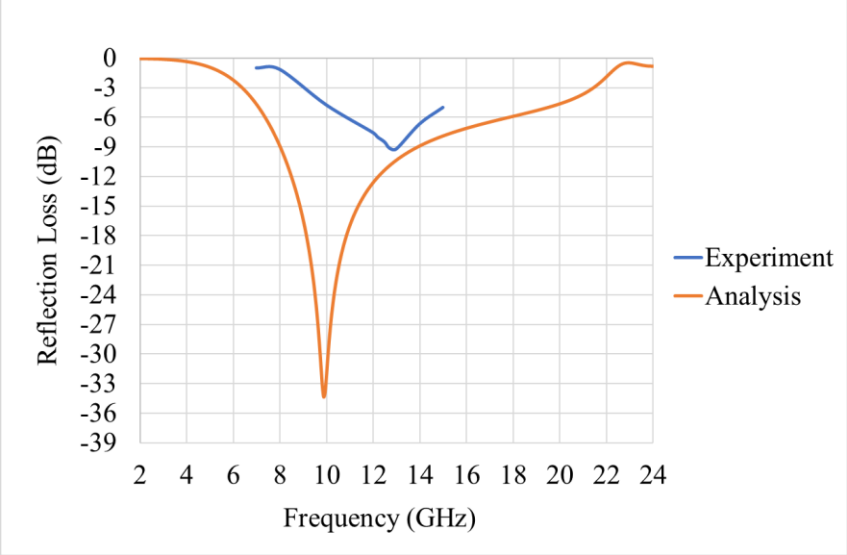

Figure 4.14 Analysis and experimental results of reflection loss for designed composite material

In order to validate the applied finite element analysis method in this study, some of the works in the literature designing FSS layer were replicated. For instance, in [39], Liu and Kim designed a radar absorbing structure having two FSS layers consisting of square loop unit cells. The first FSS layer (FSS1) had p=3.75 mm, d=3.5 mm, s=0.3, t_1=3.3 mm and the second FSS layer (FSS2) had p=7.5 mm, d=7 mm, s=0.3 mm and t_2=4.5 mm design parameters, which are shown in Figure 4.15. They have conducted an analysis in order to see the effect of surface resistance of the second FSS layer (FSS2). The same radar absorber structure together with defined surface resistances of FSS1 and FSS2 layers was analyzed using the finite element analysis method followed in this thesis study. As shown in Figure 4.16, the same result with [39] was attained.

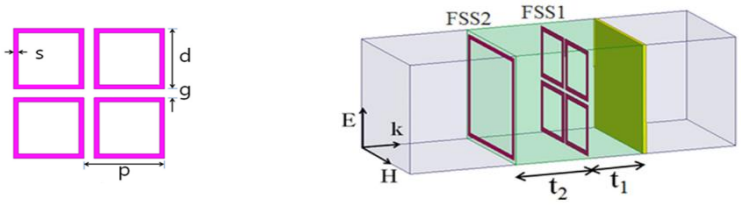

(a (b

Figure 4.15 (a) Square loop unit cell, (b) 2 layered radar absorber structure design in [39]

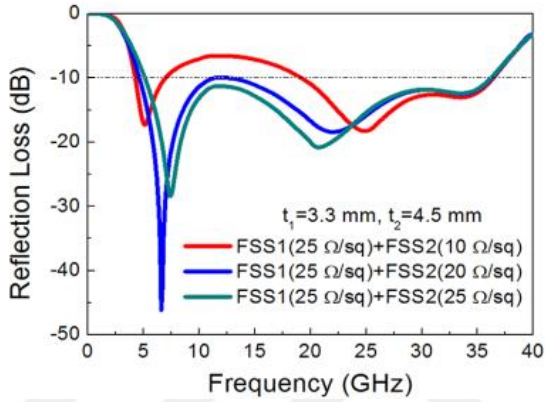

(a)

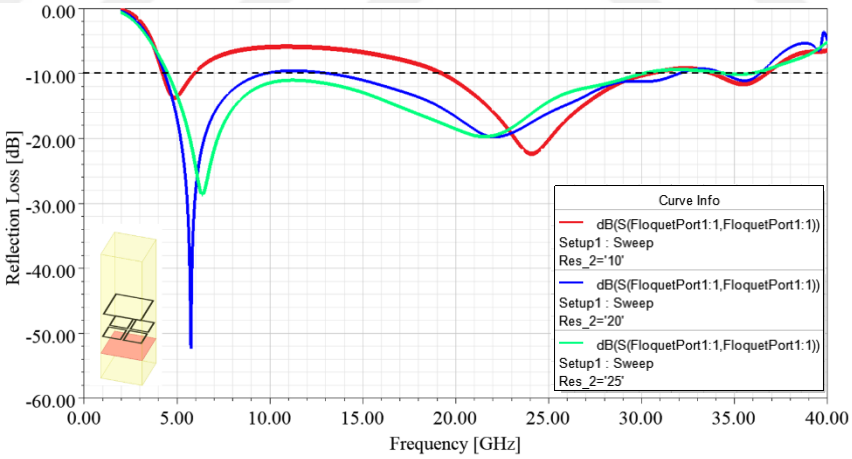

(b)

Figure 4.16 Comparison of (a) analysis result of reflection loss of the radar absorber structure designed by Liu and Kim in [39] and (b) analysis result of the same radar absorber structure by means of the finite element analysis method applied in this thesis study

Another work, which was conducted by Khan and Albert in [40], was reproduced in order to compare the analysis results. In [40], Khan and Albert were designed a rotationally symmetric element, shown in Figure 4.17, on a 0.254 mm thick dielectric substrate (Rogers RO4350B $\varepsilon_r = 3.48, \tan\delta = 0.0037$). The same structure was analyzed and result was compared with that was given in [40]. As it can be seen in Figure 4.18, the two results are matching with each other.

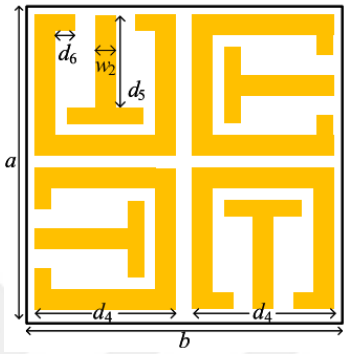

Figure 4.17 Unit cell structure designed in [40] where a=b=10 mm, d_4=4.5 mm, d_5=3.8 mm, d_6=1.0 mm, w_2=0.25 mm

Replicating the works in the literature and obtaining the same results, it was assured that finite element analysis method used in this thesis was working properly. Therefore, experimental procedure was reviewed with the aim of determining possible reasons behind small amount reflection loss and also frequency shift towards higher values (~12.5 GHz).

Size of unit cell obtained by screen printing method was measured using optical microscope (Figure 4.19.a). It was seen that 4.5 mm unit cell size and 3 mm gap sizes were achieved accurately. However, it was found that conductive ink degradation was occurred on some of the unit cells as shown in Figure 4.19.b. That may cause in increase in surface resistance locally. Also, there is waviness on the edges of unit cells due to screen printing method, which may affect inductance and capacitance behavior of FSS layer.

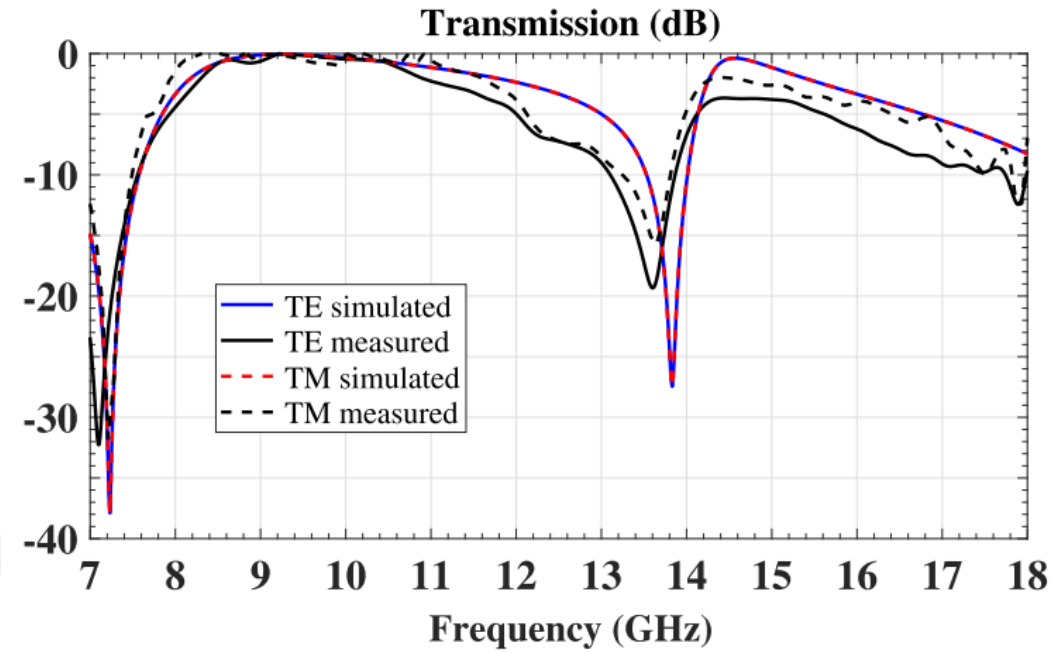

(a)

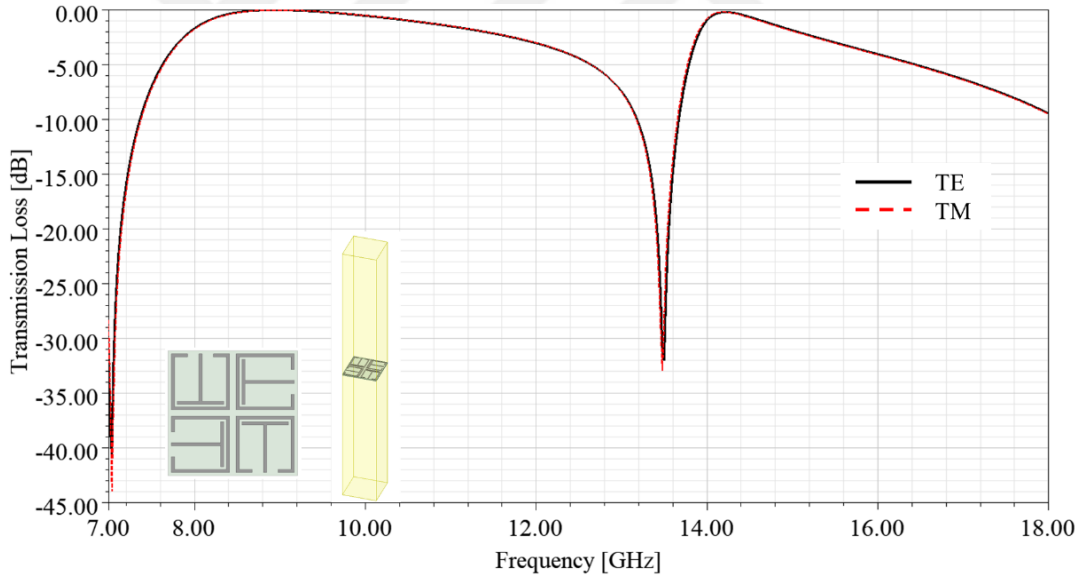

(b)

Figure 4.18 Comparison of (a) analysis result of transmission loss of the radar absorber structure designed by Khan and Albert in [39] and (b) analysis result of the same radar absorber structure by means of the finite element analysis method applied in this thesis study

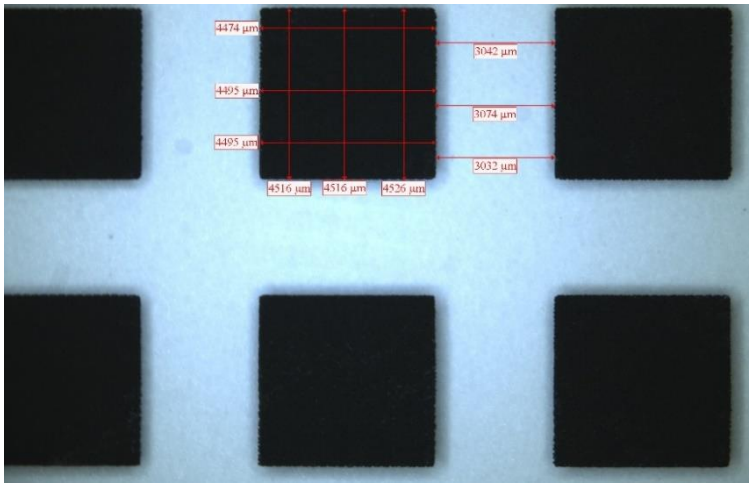

(a)

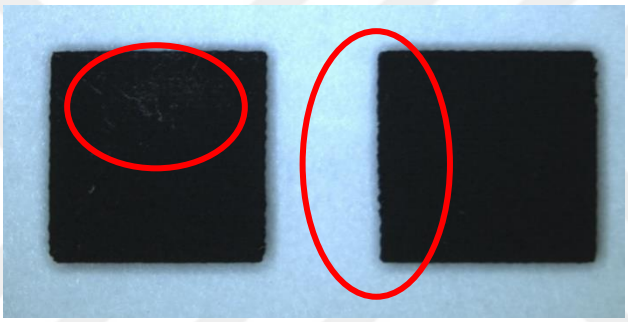

(b)

Figure 4.19 (a) Unit cell size measurement and (b) degradation and waviness detected on some of the unit cells

Considering the sensitivity analysis conducted in Chapter 2, it is strongly believed that low reflection loss and shift on resonance frequency would be caused by change in surface resistance of conductive ink and thickness of spacer.

Surface resistance of the conductive in was characterized to determine input parameters for analysis to design the composite with FSS material. To do so, measurement was applied prior to the composite plate production. There may occur a change in surface resistance as time passes between characterization process and composite plate production for experimental verification. Furthermore, surface resistance of conductive ink may be affected by heating in oven during the curing of

composite plate. In order to test that, experiment and composite plate production was repeated using the same materials. The same production steps were followed. FSS layer together with surface resistance specimens were manufactured by means of screen-printing method and composite with FSS layer was produced with prepreg lay-up technique. Specimens of surface resistance were heated in oven to represent composite curing process. Characterization of those specimens was employed before and after the heating in oven to investigate effect of heating on surface resistance. After composite plate production, thickness was measured to calculate cured ply thickness (hence spacer thickness). Finally, reflection loss behavior was determined by means of NRL Arch method.

Surface resistance measurement results, given in Table 4.12, deduced that:

- Before heating in oven, average surface resistance of the specimens was 74.15 Ω/sq, which was almost the same with the previous specimens' measurements (75.8 Ω/sq, see Table 4.1). However, comparing the variation coefficient between to specimens produced at different times, there was considerable increase in variation of measured values. This showed that as time passes surface resistance of conductive ink became unstable and had low reliability.
- After heating the specimens, average value of surface resistance increases to 90.19 Ω/sq. That means, for the analysis, surface resistance value should have been taken as 90.19 Ω/sq. Furthermore, such a high variation coefficient (27.26%) should be considered in finite element analysis. Therefore, not only average value but also minimum and maximum values of measured surface resistances, which were 56.43 Ω/sq, and 132.47 Ω/sq, should be analyzed and considered.

Table 4.12 Surface resistance measurement results of specimens before and after heating in oven for curing the composite plate

Sample Number	Before heating in oven		After heating in oven	
	ΔV/I (Ω)	R_s (Ω/sq)	ΔV/I (Ω)	R_s (Ω/sq)
1	10.05	45.55	12.45	56.43
2	11.96	54.21	14.15	64.14
3	12.41	56.25	13.93	63.15
4	15.64	70.89	17.01	77.09
5	17.88	81.06	21.83	98.94
6	24.00	108.76	29.23	132.47
7	19.82	89.82	26.27	119.06
8	16.86	76.42	23.63	107.09
9	13.78	62.46	17.11	77.55
10	25.26	114.49	25.98	117.77
11	10.71	48.54	14.11	63.96
12	11.53	52.26	14.25	64.59
13	14.02	63.54	14.26	64.65
14	15.10	68.44	17.57	79.63
15	17.11	77.55	22.04	99.91
16	21.66	98.17	27.84	126.18
17	19.77	89.6	27.05	122.60
18	17.22	78.05	20.13	91.24
19	13.11	59.42	16.84	76.31
20	19.33	87.61	22.27	100.94
Average	**16.36**	**74.15**	**19.90**	**90.19**
Standard Deviation	**4.33**	**19.64**	**5.42**	**24.58**
Variation Coefficient	**26.48%**	**26.48%**	**27.26%**	**27.26%**

Cured ply thickness of manufactured plate was determined. Thickness of PES film (0.127 mm) was subtracted from total thickness and the rest was divided in 11 since there were 10 prepreg layers to form spacer and 1 prepreg layer for top layer. As shown in Table 4.13, cured ply thickness of that composite plate was found as 0.280 mm, which was greater than that of previous one (0.261 mm, see Table 4.13),

resulting in 0.19 mm change in spacer thickness. Hence, cured ply thickness should have been taken as 0.280 mm.

Table 4.13 Cured ply thickness measurement results of the second composite with FSS layer plate

Measurement	Composite Plate Thickness (mm)	Cured Ply Thickness (mm)
1	3.17	0.277
2	3.22	0.281
3	3.20	0.279
4	3.24	0.283
5	3.23	0.282
Average	**3.21**	**0.280**
Standard Deviation	**0.03**	**0.003**
Variation Coefficient	**0.86%**	**0.9%**

As stated earlier in Chapter 2, reflection behavior of composite material is strongly affected by surface resistance and cured ply thickness (thickness of spacer material). However, it was realized that values used during design procedure and measured during experimental verification steps were not the same with each other. Therefore, attaining experimental result altered from designed composite material for radar absorption in X band (8.2 – 12.4 GHz) should be expected.

To determine amount of discrepancy between aimed reflection behavior and that of manufactured composite plate, analysis was performed for the second composite plate, considering cured ply thickness as 0.280 mm and minimum (56.43 Ω/sq), average (90.19 Ω/sq) and maximum (132.47 Ω/sq) measured surface resistances of heated specimens.

As it can be seen Figure 4.20, analysis result of manufactured composite material considerably differs from the designed composite material for radar absorption in X

band. Moreover, it could be realized that minimum, average, and maximum values of measured surface resistance had an important effect on both resonance frequency and reflection loss of composite material.

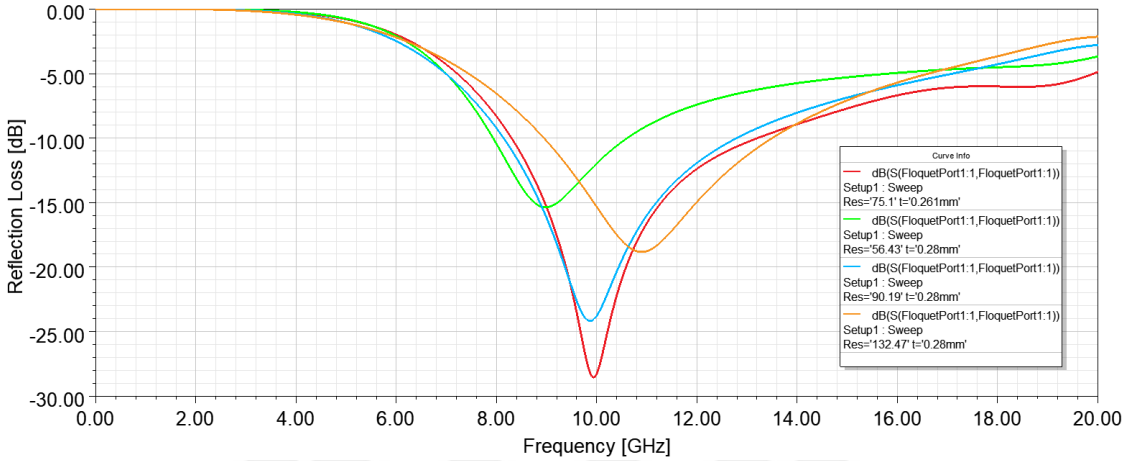

Figure 4.20 Comparison of analysis results of designed composite with FSS material (Res=75.1; t=0.261mm) and analysis of manufacture composite with FSS material applying minimum (Res=56.43; t=0.28mm), average (Res=90.19; t=0.28mm), and maximum (Res=132.47; t=0.28mm), measured surface resistance values

Reflection loss of second composite plate was characterized by means of NRL Arch method. Comparison of experiment and analysis results are shown in Figure 4.21. Also, results are tabulated in Table 4.14.

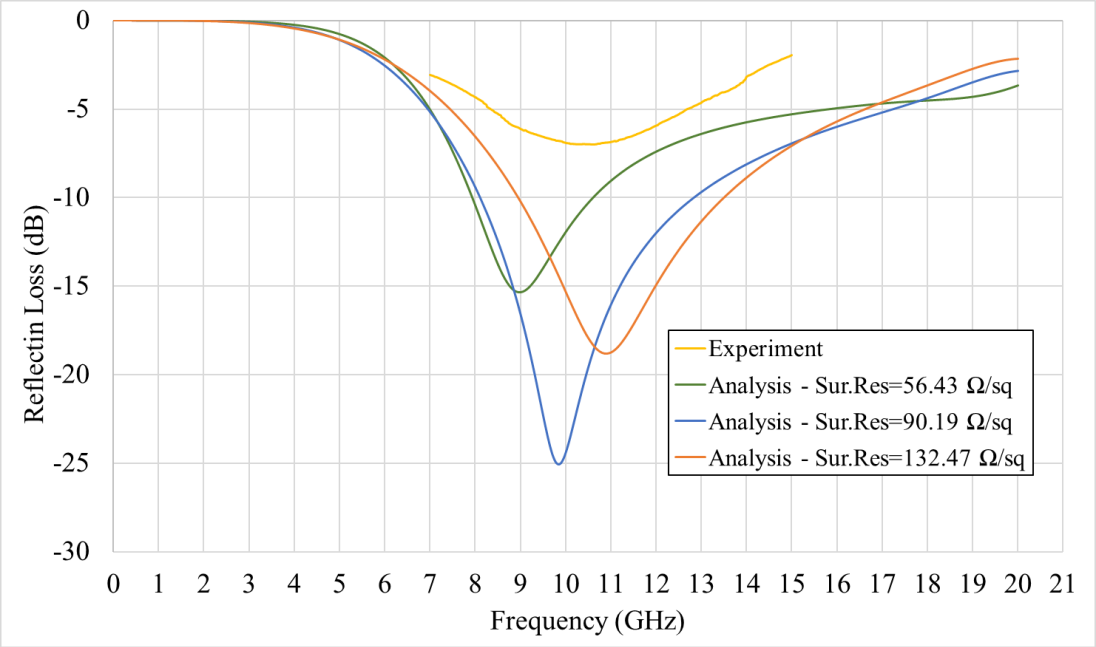

Figure 4.21 Experiment and analysis results of second manufactured composite material with FSS layer

Table 4.14 Resonance frequency and reflection loss values of experiment and analysis of designed and manufactured composite with FSS material

	Resonance Frequency (GHz)	Reflection Loss (dB)
Experiment (measurement of manufactured composite material)	10.605	-7
Analysis of designed composite material (Sur.Res=75.1 Ω/sq; t=0.261 mm)	9.88	-29.5
Analysis of manufactured composite material (Sur.Res=56.43 Ω/sq; t=0.280 mm)	9	-15
Analysis of manufactured composite material (Sur.Res=90.19 Ω/sq; t=0.280 mm)	9.85	-25
Analysis of manufactured composite material (Sur.Res=132.43 Ω/sq; t=0.280 mm)	10.9	-19

Examining Figure 4.21 and Table 4.14, it can be seen that result of experiment diverges from designed reflection loss. However, as discussed above, this situation should be expectable since two important parameters affecting reflection loss that are surface resistance and thickness of spacer material, are not the same with the aimed values. However, experimental result and analysis of manufactured composite material can be considered as similar in behavior of reflection loss curves. Although, amount of reflection loss is not the same as analyzed values, the reason behind it may be instability of conductive ink's surface resistance.

CHAPTER 5

CONCLUSION

In this thesis, a composite material having frequency selective surface was designed, manufactured and characterized. Not only radar absorption property was aimed to be designed but also processability and mechanical/thermal/physical properties were concerned. Prior to designing process, fixed parameters were defined and their values were characterized. Using fixed parameters as input variables, FSS unit cell size, periodicity and composite thickness were determined and optimized using Ansys HFSS tool by means of finite element analysis. Sensitivity analysis was conducted to see the effect of individual parameters on radar absorbing property. Scattering in fixed parameters' characterization results was taken as boundaries for sensitivity analysis in order to determine effect of measurement. It was seen that surface resistance and ply thickness (and hence spacer thickness) have an important effect on radar absorbing performance.

Screen printing method was applied to manufacture designed FSS layer, which was then, embedded between glass fiber reinforced epoxy matrix prepreg layers and cured in oven to produce composite material. With this approach, it was aimed to have a composite material having both convenient structural properties and also radar absorbing performance.

In order to confirm that mechanical/thermal/physical properties of composite with FSS layer material were suitable as a structural member, characterization tests were applied. It was concluded that presence of FSS layer fabricated on PES film slightly decreases the mechanical properties of composite material, in which amount of deterioration can be considered as acceptable. However, failure behavior of composite material was completely altered such that delamination at the interface of

PES film layer was occurred. Although structural parts are designed with high factor of safety in such a way that failure of material can never happen, failure behavior of composite with FSS material should be improved. To do so, woven glass fiber fabric can be used as substrate for FSS structure to be printed on. With this way, once glass fiber fabric is placed between prepreg layers, excess resin can flow and impregnate the fabric during oven curing so that fabric is consolidated with composite material. As a future work, FSS layer printed on glass fiber fabric can be applied to improve structural properties of composite material.

Designed composite having FSS layer material was manufactured and tested by means of NRL Arch method. It was seen that there is a significant deviation between analysis and experimental results. To be sure about followed analysis method, some of the literature works were replicated. Results were compared and it was observed that they are compatible with each other. Therefore, it was concluded that analysis method was not the reason behind deviation of experiment from analysis. Considering the sensitivity analysis, this deviation may be caused by alteration in surface resistivity of conductive ink and/or cured ply thickness. There was a time lag between performing analysis to design of composite material and production for experimental verification. Surface resistance of conductive ink may be changed as time passes. Also, it may be influenced by heating in oven during composite plate curing process. In order to examine them, experimental procedure was repeated. Specimens for characterization of surface resistance was manufactured again and heated in oven. Measurement results of before and after heating in oven showed that heated specimens had higher surface resistance. Moreover, there was a huge variation coefficient of measured results, which increased considerably as time passes. Those conclusions revealed that there was a significant instability in conductive ink. Thickness of manufactured composite plate was also measured. It was seen that thickness of composite plate was thicker (0.212 mm) from the aimed value. As a result, discrepancy between experimental result and analysis of designed material can be considered as expectable since two design parameters (surface resistance and spacer thickness) were not the same with the aimed values. Therefore,

as a future work, experimental process can be conducted with stable conductive ink and a unit cell having low sensitivity for cured play thickness can be designed.

REFERENCES

[1] Li, H.-J., & Kiang, Y.-W. (2005). Radar and Inverse Scattering. *The Electrical Engineering Handbook* (pp. 671–690). Elsevier Academic Press.

[2] Micheli, D., Apollo, C., Pastore, R., & Marchetti, M. (2010). X-Band microwave characterization of carbon-based nanocomposite material, absorption capability comparison and RAS design simulation. *Composites Science and Technology, 70*(2), 400-409. doi:10.1016/j.compscitech.2009.11.015

[3] Duan, Y., & Guan, H. (2017). Hybrid Microwave Absorbers. In *Microwave Absorbing Materials* (p. 190). Pan Stanford Publishing.

[4] Kim, J. (2012). Broadband radar absorbing structures of car1bon nanocomposites. *Advanced Composite Materials, 21*(4), 333-344. doi:10.1080/09243046.2012.736350

[5] Shin, J., Jang, H., Choi, W., Song, T., Kim, C., & Lee, W. (2015). Design and verification of a single slab RAS through mass production of glass/MWNT added epoxy composite prepreg. *Journal of Applied Polymer Science, 132*(22). doi:10.1002/app.42019

[6] Kim, S., & Kim, S. (2018). Design of Radar Absorbing Structures Utilizing Carbon-Based Polymer Composites. *Polymers and Polymer Composites, 26*(1), 105-110. doi:10.1177/096739111802600113

[7] Wang, H., & Zhu, D. (2018). Double layered radar absorbing structures of Silicon Carbide fibers/polyimide composites. *Synthetic Metals, 246*, 213-219. doi:10.1016/j.synthmet.2018.10.020

[8] Meng, W., Yuping, D., Shunhua, L., Xiaogang, L., & Zhijiang, J. (2009). Absorption properties of carbonyl-iron/carbon black double-layer microwave absorbers. *Journal of Magnetism and Magnetic Materials, 321*(20), 3442-3446. doi:10.1016/j.jmmm.2009.06.040

[9] Ismail, I., Ibrahim, I. R., Matori, K. A., Awang, Z., Zulkimi, M. M., Idris, F. M., Nazlan, R., Azis R.S., Zaid, M. H. M., Rusly, S. N. A., Ertugrul, M. (2020). Comparative study of single- and double-layer BaFe12O19-Graphite nanocomposites for electromagnetic wave absorber applications. *Materials Research Bulletin, 126*, 110843. doi:10.1016/j.materresbull.2020.110843

[10] Melvin, G. J., Ni, Q., Suzuki, Y., & Natsuki, T. (2014). Microwave-absorbing properties of silver nanoparticle/carbon nanotube hybrid nanocomposites. Journal of Materials Science, 49(14), 5199-5207. doi:10.1007/s10853-014-8229-9

[11] Cao, M., Yang, J., Song, W., Zhang, D., Wen, B., Jin, H., Hou, Z., Yuan, J. (2012). Ferroferric Oxide/Multiwalled Carbon Nanotube vs Polyaniline/Ferroferric Oxide/Multiwalled Carbon

Nanotube Multiheterostructures for Highly Effective Microwave Absorption. *ACS Applied Materials & Interfaces, 4*(12), 6949-6956. doi:10.1021/am3021069

[12] Bateer, B., Wang, X., Tian, C., Xie, Y., Pan, K., Ping, W., & Fu, H. (2020). Ni2P nanocrystals coated on carbon nanotubes as enhanced lightweight electromagnetic wave absorbers. *Carbon, 161*, 51-61. doi:10.1016/j.carbon.2019.12.061

[13] Li, Z., Wang, X., Ling, H., Lin, H., Wang, T., Zhang, M., Meng, A., Li, Q. (2020). Electromagnetic wave absorption properties of SiC@SiO2 nanoparticles fabricated by a catalyst-free precursor pyrolysis method. *Journal of Alloys and Compounds, 830,* 154643. doi:10.1016/j.jallcom.2020.154643

[14] Balanis, C. A. (2012). *Advanced Engineering Electromagnetics (2nd ed.)*. John Wiley and Sons.

[15] Bain, A. K., & Chand, P. (2017). *Ferroelectrics: Principles and Applications.* John Wiley & Sons.

[16] Fulay, P., & Lee, J.-K. (2010). *Electronic, Magnetic, and Optical Materials.* CRC Press.

[17] Tiwari, A., & Valyukh, S. (Eds.). (2014). *Advanced Energy Materials.* John Wiley & Sons, Inc. Hoboken. doi: 10.1002/ente.201500283

[18] Sahay, K. (2006). *Basic Concepts of Electrical Engineering.* New Age International.

[19] Morrish, A.H. (2001). *The Physical Principles of Magnetism.* IEEE Press.

[20] Watts, C. M., Liu, X., & Padilla, W. J. (2012). Metamaterial Electromagnetic Wave Absorbers. *Advanced Materials, 24*(23). doi:10.1002/adma.201200674

[21] Folgueras, L. D., & Rezende, M. C. (2008). Multilayer radar absorbing material processing by using polymeric nonwoven and conducting polymer. *Materials Research, 11*(3), 245-249. doi:10.1590/s1516-14392008000300003

[22] Costa, F., Monorchio, A., & Manara, G. (2016). Theory, design and perspectives of electromagnetic wave absorbers. *IEEE Electromagnetic Compatibility Magazine, 5*(2), 67-74. doi:10.1109/memc.0.7543954

[23] Jacard, B., Valenzuela, A., & Gonzalez, M. (2018). Practical Universal Method for Designing Single-Layer Electromagnetic Wave Absorbers. *Open Journal of Antennas and Propagation, 06*(04), 84-92. doi:10.4236/ojapr.2018.64008

[24] Saville, P. (2007). *Optimisation of Dallenbach Layers using Real Materials* (Tech. No. DRDC Atlantic TM 2007-012). Defence R&D Canada – Atlantic.

[25] Tong, X. C. (2009). Microwave Absorber Materials. In *Advanced Materials and Design for Electromagnetic Interference Shielding* (pp. 240-242). CRC Press.

[26] Yuzcelik, C. K. (2003). *Radar Absorbing Material Design* [Master's thesis, Naval Postgraduate School]. NPS Archive: Calhoun. https://calhoun.nps.edu/handle/10945/6246

[27] Rana, S. A., Mao, L., & Ning, H. (2018). Frequency Selective Surfaces: A Review. *Applied Sciences*, *8*(1689). doi:10.3390/app8091689

[28] Narayan, S., Sangeetha, B., & Jha, R. M. (2016). *Frequency Selective Surfaces based High Performance Microstrip Antenna* (pp. 3–4). SpringerBriefs in Electrical and Computer Engineering. doi:10.1007/978-981-287-775-8

[29] Fallah, M., Ghayekhloo, A., & Abdolali, A. (2015). Design of frequency selective band stop shield using analytical method. *Journal of Microwaves, Optoelectronics and Electromagnetic Applications*, *14*(2), 217–228. https://doi.org/10.1590/2179-10742015v14i2536

[30] Silva, M. W., Kretly, L. C., & Barbin, S. E. (2014). Practical guidelines for the design and implementation of microwave absorber using FSS-frequency selective surfaces. *2014 20th International Conference on Microwaves, Radar and Wireless Communications (MIKON)*. https://doi.org/10.1109/mikon.2014.6899866

[31] Liu, T., & Kim, S.-S. (2016). Design of wide-bandwidth electromagnetic wave absorbers using the inductance and capacitance of a square loop-frequency selective surface calculated from an equivalent circuit model. *Optics Communications*, *359*, 372–377. https://doi.org/10.1016/j.optcom.2015.10.011

[32] Marcuvitz, N. (1951). In *Waveguide Handbook* (pp. 280–290). McGraw-Hill.

[33] Liu, T., & Kim, S. S. (2019). High-capacitive frequency selective surfaces of folded spiral conductor arrays. *Microwave and Optical Technology Letters*, *62*(1), 301–307. https://doi.org/10.1002/mop.32006

[34] Baek, S. M., Lee, W. J., & Joo, Y. S. (2017). A study on a radar absorbing structure for Aircraft Leading Edge Application. *International Journal of Aeronautical and Space Sciences*, *18*(2), 215–221. https://doi.org/10.5139/ijass.2017.18.2.215

[35] Begaud, X., Lepage, A., Varault, S., Soiron, M., & Barka, A. (2018). Ultra-wideband and wide-angle microwave metamaterial absorber. *Materials*, *11*(10), 2045. https://doi.org/10.3390/ma11102045

[36] Ramezani Varkani, A., Hossein Firouzeh, Z., & Zeidaabadi Nezhad, A. (2018). Equivalent circuit model for array of circular loop FSS structures at oblique angles of incidence. *IET Microwaves, Antennas & Propagation*, *12*(5), 749–755. https://doi.org/10.1049/iet-map.2017.1004

[37] Naftaly, M., Das, S., Gallop, J., Pan, K., Alkhalil, F., Kariyapperuma, D., Constant, S., Ramsdale, C., & Hao, L. (2021). Sheet resistance measurements of conductive thin films: A comparison of techniques. *Electronics*, *10*(8), 960. https://doi.org/10.3390/electronics10080960

[38] Firouzfar, A., Afsahi, M., & Orouji, A. A. (2019). Novel synthesis formulas to design square patch frequency selective surface absorber based on equivalent circuit model. *International Journal of RF and Microwave Computer-Aided Engineering*, *29*(6). https://doi.org/10.1002/mmce.21680

[39] Liu, T., & Kim, S.-S. (2018). Design of ultra wide-bandwidth double-layer electromagnetic wave absorbers with square-loop frequency selective surfaces. *Microwave and Optical Technology Letters*, *60*(8), 2013–2018. https://doi.org/10.1002/mop.31287

[40] Khan, S., & Eibert, T. F. (2018). A multifunctional metamaterial-based dual-band isotropic frequency-selective surface. *IEEE Transactions on Antennas and Propagation*, *66*(8), 4042–4051. https://doi.org/10.1109/tap.2018.2835667